NASA CONTRACTOR REPORT

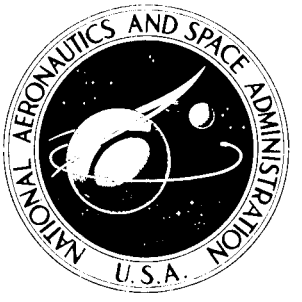

NASA CR-1789

NASA CR-1789

A STUDY TO DETERMINE THE FLIGHT CHARACTERISTICS AND HANDLING QUALITIES OF VARIABLE GEOMETRY SPACECRAFT

Volume II — Medium L/D Concept With Switch-Blade Wings

by B. J. Kuchta and G. R. Friedman

Prepared by
CONVAIR DIVISION OF GENERAL DYNAMICS
San Diego, Calif. 92112
for Langley Research Center

NATIONAL AERONAUTICS AND SPACE ADMINISTRATION • WASHINGTON, D. C. • MARCH 1972

1. Report No.	2. Government Accession No.	3. Recipient's Catalog No.
NASA CR-1789		

4. Title and Subtitle	5. Report Date
A STUDY TO DETERMINE THE FLIGHT CHARACTERISTICS AND HANDLING QUALITIES OF VARIABLE GEOMETRY SPACECRAFT - VOLUME II - MEDIUM L/D CONCEPT WITH SWITCH-BLADE WINGS	March 1972
	6. Performing Organization Code

7. Author(s)	8. Performing Organization Report No.
B. J. Kuchta and G. R. Friedman	GDC-DDE68-003
	10. Work Unit No.

9. Performing Organization Name and Address	11. Contract or Grant No.
General Dynamics Convair Division P. O. Box 1128 San Diego, CA 92112	NAS1-7971
	13. Type of Report and Period Covered
12. Sponsoring Agency Name and Address	Contractor Report
National Aeronautics and Space Administration Washington, DC 20546	14. Sponsoring Agency Code

15. Supplementary Notes

16. Abstract

Flight characteristics and wing deployment transients for a variable geometry logistics spacecraft concept having a hypersonic lift-drag ratio near 2.0, and employing switch-blade wings for deployment at high subsonic-transonic speeds have been determined. These characteristics are based on detailed static wind tunnel results and estimated weight and inertial characteristics of a 9-man logistics lifting entry vehicle. In all instances, unpowered flight is assumed. The present volume is the second of a four volume series encompassing hypersonic lift-drag ratio vehicles from about 1 to 3, and including several forms of deployable lifting surfaces.

17. Key Words (Suggested by Author(s))	18. Distribution Statement
Dynamic Stability Handling Qualities Manned Spacecraft Variable Geometry	Unclassified - Unlimited

19. Security Classif. (of this report)	20. Security Classif. (of this page)	21. No. of Pages	22. Price*
Unclassified	Unclassified	69	$3.00

*For sale by the National Technical Information Service, Springfield, Virginia 22151

TABLE OF CONTENTS

LIST OF FIGURES

LIST OF FIGURES, Contd

LIST OF TABLES

LIST OF SYMBOLS

b	Aerodynamic reference span, ft
C_D	Drag coefficient
C_L	Lift coefficient
$C_{1/2}$	Cycles to one-half amplitude
C_{ℓ_β}	Lateral stability parameter
C_m	Pitching moment coefficient
C_{n_β}	Directional stability parameter
C_p	Center of pressure
C_{Y_β}	Side force parameter
c	Wing chord, ft
c.g.	Center of gravity percent of actual body length
g	Gravity, 32.2 ft/sec^2
h	Height of body at Station X, ft
H	Altitude, ft
I_{xx}	Moment of inertia about X body axis, slug-ft^2
I_{xz}	Cross product of inertia, slug-ft^2
I_{yy}	Moment of inertia about Y body axis, slug-ft^2
I_{zz}	Moment of inertia about Z body axis, slug-ft^2
i_w	Wing incidence angle

K	Constant
K_P	Roll rate gain
K_Q	Pitch rate gain
K_R	Yaw rate gain
L	Rolling moment, ft-lb
ℓ	Aerodynamic reference length, ft
M	Pitching moment, ft-lb
N	Yawing moment, ft-lb
n_z	Normal load factor, g
n_z/α	Steady-state normal acceleration per radian of angle of attack
P, p	Rolling rate, rad/sec
P_s	Stability axis roll rate, rad/sec
$\bar{Q}$	Free stream dynamic pressure, psf
Q, q	Pitching rate, rad/sec
R, r	Yawing rate, rad/sec
R_s	Stability axis yaw rate, rad/sec
S	Aerodynamic reference area, ft^2
s	Laplace operater
t	Time, sec
$t_{1/2}$	Time to one-half amplitude, sec
U_B	Body velocity along body X axis
V	Free stream velocity, ft/sec

V_B	Body velocity along body Y axis
W_B	Body velocity along body Z axis
X	Longitudinal distance along body, downrange, ft
X_s	Acceleration along the X stability axis, ft/sec^2
Y	Spanwise, ft
Y_s	Acceleration along the Y stability axis, ft/sec^2
y_u	Wing upper surface ordinate, ft
y_ℓ	Wing lower surface ordinate, ft
Z_s	Acceleration along the Z stability axis, ft/sec^2
α	Angle of attack, deg
β	Angle of side slip, deg
γ	Flight path angle, deg
δ_a	Aileron deflection, deg
δ_e	Elevator or elevon deflection, deg
δ_r	Rudder deflection, deg
ζ	Relative damping factor
ρ	Air density, slugs/ft^3
ϕ	Euler roll angle, deg
ψ	Euler yaw angle, deg

θ	Euler pitch angle, deg
$\Lambda_{C/2}$	Wing half chord sweep angle, deg
Σ	Summation
$\omega^2_{n_{sp}}$	Short-period natural frequency
$\partial(\ )/\partial(\ )$	Partial derivative
$\dot{(\ )}$	$\frac{d(\ )}{dt}$

Subscripts

e	Equivalent velocity
W	Portion due to wing
x	Longitudinal distance
z	Vertical distance
0	Conditions at zero angle of attack
P	Pilot

SUMMARY

A study was conducted to determine the flight characteristics and wing deployment transients for a variable geometry logistics spacecraft concept having a hypersonic lift-drag ratio near 2.0, and employing switchblade wings for deployment at transonic speeds. Unpowered flight conditions are considered throughout the study. The body of the spacecraft is elliptical in cross section and horizontal stabilizers and a vertical tail are located near the base of the body to provide longitudinal and directional stability. Highly cambered high aspect ratio wings are stowed on top of the body and deployed at transonic speeds at altitudes between 35,000 and 45,000 feet to a 15° half-chord sweep condition. Deployment in this altitude range retains enough dynamic pressure for control while permitting enough time for satisfactory high L/D maneuvering.

Detailed static wind tunnel aerodynamic data obtained from hypersonic to low subsonic speeds were used to estimate the dynamic aerodynamic stability characteristics throughout the entire entry flight regime. The aerodynamic data are presented as total vehicle derivatives with the wing stowed, and as wing increment derivatives which are added to the stowed wing values. The wing increments are presented for various wing sweep positions.

The spacecraft concept studied is dynamically stable throughout the flight envelope, but stability augmentation is required to provide acceptable handling qualities with the vehicle center of gravity located at 60.1 percent of the actual body length. The stability augmentation recommended is of the simple rate feedback type with gain scheduling. The rudder as now designed is deficient for yaw damping. However, the design of a larger rudder poses no problems. The dihedral in the horizontal tail results in excessive proverse yaw at transonic speeds and adverse yaw above Mach 2.5 when differential tail is used for roll control. The excessive adverse yaw at Mach numbers above 3 in conjunction with the rudder make it impossible to generate separate yaw and roll moments needed for augmentation. It is worth considering a variable dihedral tail for any flight research vehicle based on this concept.

The piloting task during wing deployment consists of a simple push-over maneuver. However, maintaining the vehicle in a low angle of attack is recommended. Wing deployment starts at Mach 0.95 and complete deployment is accomplished at Mach 0.5. The incremental nose down pitching moment produced by wing deployment helps keep the vehicle near constant C_L.

Landing characteristics of this spacecraft concept are comparable to present day high performance fighter aircraft. The approach speed is in the 180-190 knot range with an 8° flight path angle. The flare is initiated at about 300 feet of altitude, and flare load factor is approximately 0.15g.

A STUDY TO DETERMINE THE FLIGHT CHARACTERISTICS AND HANDLING QUALITIES OF VARIABLE GEOMETRY SPACECRAFT

by B. J. Kuchta and G. R. Friedman

Convair Division of General Dynamics Corporation
San Diego, California

SECTION 1

INTRODUCTION

Considerable effort is at present being devoted to the development of lifting entry spacecraft concepts for use as possible logistics systems with lift-drag ratios varying from near 1.0 to in excess of 3.0. Recent studies related to the development of hypersonic lifting bodies, optimized with regard to improved aerodynamic performance, have shown that body shapes of moderate fineness ratios having relatively good volume to wetted area relationships (and hence, lower weight) can provide hypersonic lift-to-drag ratios of up to approximately 3.5. (See Reference 1.)

For vehicles conceived to be piloted or flown in the conventional sense during the entire entry and to land in the manner of aircraft, aerodynamic features must be tailored for both hypersonic and low-subsonic flight. The moderate-to-high lift-to-drag ratio hypersonic lifting body vehicles have unacceptable subsonic performance for horizontal landing without modification or compromise to the basic shape. The incorporation of some form of deployable lifting surface offers a possible means of providing efficient subsonic land recovery, while retaining the desired hypersonic shape. If manned spaceflight is to become a routine operation, independent of massive sea recovery logistics, the desirability of landing at one of several preselected sites with a minimum of ground support requirements must become a reality.

The purpose of this investigation is to provide information by use of static wind tunnel data input into the simulator to study handling qualities and the overall dynamic stability and control, wing deployment characteristics, and landing characteristics of a spacecraft concept having a hypersonic lift-drag ratio of approximately 2.0. The spacecraft concept incorporates switch-blade wings as a variable geometry feature to improve subsonic aerodynamic characteristics.

The investigation incorporated both analytical analysis and simulation. The analytical analysis provided information as to handling qualities relative to both longitudinal and

lateral modes, period and damping. The simulation provided a vehicle by which a flight could be flown from 100,000 feet altitude, through wing deployment, to touchdown.

The results of the investigation are presented in the form of time histories, periods, damping, and time to damp to one-half amplitude of the longitudinal and lateral oscillations. Where possible, the results are discussed in terms of handling qualities parameters which are in current usage for proposed entry vehicle configurations and high performance aircraft. The sign convention used is presented in Figure 1-1.

SECTION 2

VEHICLE DESCRIPTION

The spacecraft concept investigated has a body with modified elliptical cross section and an area distribution which represents a minimum wave-drag shape modified by nose bluntness at hypersonic speeds as determined under the geometric constraints of length and volume. (See Reference 1.) Horizontal stabilizers and a vertical tail are located near the base of the body to provide longitudinal and directional stability. High aspect ratio wings having a thick, highly cambered airfoil section are stowed on top of the body during entry and are deployed at subsonic speeds to a 15° sweep condition. Elevon controls are located on the horizontal stabilizers to provide longitudinal control, and roll control when differentially deflected. Rudder controls are located on the vertical tail to provide directional control.

A drawing of the complete spacecraft is shown in Figure 2-1. Table 2-1 presents body ordinates normalized with respect to length and Table 2-2 presents wing airfoil section ordinates normalized with respect to chord. Figure 2-2 shows the details of the wing.

The wing panel is an approximately 18-percent thick, highly cambered, St. Cyr (Royer 156) airfoil section measured parallel to the airstream at zero degree sweep of the half chord. The wing taper ratio is 0.75 and its aspect ratio is 9.42 based on its own projected wing planform area. The projected planform area is 30.1 percent of the body planform area. The wing incidence angle is 4 degrees, relative to wing ordinate reference line. See Figure 2-2.

The horizontal stabilizers, set at 30 degrees of dihedral angle, are located along the body lower surface ridge line just ahead of the base. The stabilizers, which are 2-degree (included angle) wedge airfoil sections, have a 65-degree leading edge sweep. The elevon control surfaces used for pitch and roll control are located at the trailing edge of the stabilizers. Total exposed horizontal stabilizer area including the elevons is 20.0 percent of the body planform area.

A single centerline vertical tail is located on the body and a rudder is located at the trailing edge for yaw control.

The sizing of the spacecraft concept being considered was performed in a study entitled Weight and Performance Characteristics of Variable-Geometry Spacecraft, which was conducted at Convair under contract NAS1-7675. The results of that study indicate that the spacecraft inertia characteristics with wing stowed should be:

Weight	15,170 lb
c.g.	0.601ℓ
I_{xx}	6,070 slug-ft^2
I_{yy}	49,950 slug-ft^2
I_{zz}	52,950 slug-ft^2
I_{xz}	500 slug-ft^2

Reference dimensional data for reducing the aerodynamic characteristics to coefficient form are:

Length (ℓ)	37.6 feet
Span (b)	11.2 feet
Area (S)	297 feet^2

All of the above data is used throughout the analysis and simulation.

Table 2-1. Design Body Ordinates

Body Station, x/ℓ	Planview, Lateral Ordinate (Semimajor Axis), y/ℓ	Vertical Ordinate Below Body-ordinate Reference Line, z/ℓ
0.0000	0.0000	0.0000
0.0050	0.0032	0.0032
0.0100	0.0055	0.0055
0.0200	0.0098	0.0098
0.0300	0.0136	0.0136
0.0400	0.0170	0.0170
0.0500	0.0202	0.0202
0.0600	0.0231	0.0231
0.0800	0.0284	0.0284
0.1000	0.0333	0.0333
0.1500	0.0441	0.0441
0.2000	0.0538	0.0538
0.3000	0.0715	0.0715
0.4000	0.0870	0.0870
0.5000	0.1005	0.1005
0.6000	0.1121	0.1121
0.7000	0.1221	0.1221
0.8000	0.1305	0.1295
0.9000	0.1369	0.1288
1.0000	0.1402	0.1225

Table 2-2. Wing Ordinates

x/c	y_u/c	y_L/c
0.013	0.038	-0.027
0.025	0.052	-0.034
0.050	0.074	-0.040
0.075	0.091	-0.044
0.100	0.105	-0.044
0.150	0.127	-0.038
0.200	0.144	-0.030
0.300	0.163	-0.014
0.400	0.166	0.001
0.500	0.160	0.018
0.600	0.144	0.030
0.700	0.116	0.032
0.800	0.083	0.030
0.900	0.045	0.018
0.950	0.026	0.010
1.000	0	0

SECTION 3

AERODYNAMIC DATA

This section is a discussion of the aerodynamic characteristics with the wing fully stowed ($\Lambda = 90°$) and with the wing at various deployed positions. Static wind tunnel aerodynamic data were used in the form of linear tables with Mach number as the independent variable. In order to include the angle of attack non-linearities, first and second order partials of each aerodynamic derivative were derived from the measured wind tunnel data. A major effort was expended in the development of the aerodynamic data because any stability and control analysis or simulation of an aerodynamic vehicle is only as good as the aerodynamic data used.

The wind tunnel measured data consisted of static aerodynamic coefficients for the complete configuration, body alone, horizontal stabilizer-body, horizontal stabilizer-body vertical tail and body-horizontal stabilizer-vertical tail. With this type of breakdown the influence of each component could be derived. Since this study depended upon dynamic derivatives, a method was developed whereby dynamic derivatives could be obtained from the static component aerodynamic data and geometric considerations.

The wind tunnel test data were available at Mach numbers of 0.3, 0.5, 0.80, 0.90, 0.95, 1.00, 1.20, 2.30, 2.96, 3.96, 4.63, and 10.0. At each Mach number C_D, C_L, C_m, C_{Y_β}, C_{n_β} and C_{ℓ_β} were available as a function of angle of attack and several elevon deflections. The angle of attack range generally was from about -2 degrees to 18 degrees. Data was taken from 20° to -30° of elevon deflection.

Figures 3-1 through 3-29 present all of the reduced aerodynamic data as a function of Mach number. All moment coefficients that were obtained from NASA are referenced to 52.5 percent of the longitudinal length (ℓ) and were transferred to the vehicle center of gravity located at 60.1 percent of the length for all computations of handling qualities parameters and flight characteristics in this document. For a detailed discussion of each coefficient, see Reference 2.

In order to improve the subsonic characteristic of the spacecraft concept, the switchblade wings are deployed at transonic speeds. The altitude and Mach number time history for deployment are to be determined in this study. Low speed wind tunnel tests were conducted at Mach numbers from 0.30 to 0.95. Since tests were made with and without the wing, downwash on the tail surfaces induced by the wing was determined directly from wind tunnel data.

The wind tunnel aerodynamic data were reduced in a manner which allows the wing effects to be considered as increments which, when the wing is deployed, are algebraically added to the spacecraft without wing data. With regard to the simulator, this method of data handling simplifies the generation of the aerodynamic coefficients during wing deployment and thereafter.

Figures 3-30 through 3-32 present the wing incremental aerodynamic data as a function of angle of attack and wing sweep angle. Wind tunnel tests were conducted at 15°, 30°, 45°, 60°, and 75° of wing sweep.

At a given Mach number all of the non-dimensionalized coefficients are evaluated. Since what is needed for the six-degree-of-freedom equations of motion are six non-dimensionalized coefficients, the following equations present the combining equations.

$$C_D = C_{D_0} + \frac{\partial C_D}{\partial \alpha^2} \alpha^2 + \frac{\partial C_D}{\partial \delta_e^2} \delta_e^2 \tag{1}$$

$$C_L = C_{L_0} + C_{L_\alpha} \alpha + \frac{\partial C_{L_\alpha}}{\partial \alpha} \alpha^2 + C_{L_{\delta_e}} \delta_e + \frac{\partial C_{L_{\delta_e}}}{\partial \alpha} \alpha \delta_e + C_{L_q} \frac{\ell}{2V} q \tag{2}$$

$$C_m = C_{m_0} + C_{m_\alpha} \alpha + \frac{\partial C_{m_\alpha}}{\partial \alpha} \alpha^2 + C_{m_{\delta_e}} \delta_e + \frac{\partial C_{m_{\delta_e}}}{\partial \alpha} \alpha \delta_e + C_{m_q} \frac{\ell}{2V} q \tag{3}$$

$$C_Y = C_{Y_\beta} \beta + \frac{\partial C_{Y_\beta}}{\partial \alpha} \alpha \beta + C_{Y_r} \frac{b}{2V} r + C_{Y_p} \frac{b}{2V} p + C_{Y_{\delta_r}} \delta_r + \frac{\partial C_{Y_{\delta_r}}}{\partial \alpha} \alpha \delta_r \tag{4}$$

$$C_n = C_{n_\beta} \beta + \frac{\partial C_{n_\beta}}{\partial \alpha} \alpha \beta + C_{n_r} \frac{b}{2V} r + C_{n_p} \frac{b}{2V} p + \frac{\partial C_{n_p}}{\partial \alpha} \alpha \frac{b}{2V} p + C_{n_{\delta_r}} \delta_r + \frac{\partial C_{n_{\delta_r}}}{\partial \alpha} \alpha \delta_r + C_{n_{\delta_a}} \delta_a \tag{5}$$

$$C_{\ell} = C_{\ell_\beta}\,\beta + \frac{\partial C_{\ell_\beta}}{\partial \alpha}\,\alpha\,\beta + C_{\ell_r}\,\frac{b}{2V}\,r + C_{\ell_p}\,\frac{b}{2V}\,p + C_{\ell_{\delta_a}}\,\delta_a + \frac{\partial C_{\ell_{\delta_a}}}{\partial \alpha}\,\alpha\,\delta_a$$

$$+ C_{\ell_{\delta_r}}\,\delta_r + \frac{\partial C_{\ell_{\delta_r}}}{\partial \alpha}\,\alpha\,\delta_r \qquad (6)$$

SECTION 4

SIMULATION

The following equations represent six degree-of-freedom equations of motion about a system of body oriented axes. The aerodynamic coefficients used in the equations are those described in Section 3 of this report. The force equations are wind-axis oriented and the moment equations are body-axis oriented.

The velocity equation is

$$\dot{V} = X_s \cos\beta + Y_s \sin\beta \tag{7}$$

The angle of attack equation is

$$\dot{\alpha} = Q + \frac{\left(\frac{Z_S}{V} - P_s \sin\beta\right)}{\cos\beta} \tag{8}$$

where

$$P_s = P\cos\alpha + R\sin\alpha \tag{9}$$

The side-slip angle equation is

$$\dot{\beta} = \frac{(Y_s \cos\beta - X_s \sin\beta)}{V} - R_s \tag{10}$$

where

$$R_s = R\cos\alpha - P\sin\alpha \tag{11}$$

The force equations are

$$X_s = g_{x_B}\cos\alpha + g_{z_B}\sin\alpha - C_D \bar{Q}\left(\frac{S}{m}\right) \tag{12}$$

$$Y_s = g_{y_B} + C_Y \bar{Q}\,\frac{S}{m} \tag{13}$$

$$Z_s = g_{z_B}\cos\alpha - g_{x_B}\sin\alpha - C_L \bar{Q}\left(\frac{S}{m}\right) \tag{14}$$

The body gravity components are

$$g_{x_B} = -g \sin\theta \tag{15}$$

$$g_{y_B} = g \cos\theta \sin\phi \tag{16}$$

$$g_{z_B} = g \cos\theta \cos\phi \tag{17}$$

Altitude and ground track computations are made by resolving the total velocity V into body-axis components by the equations

$$U_B = V \cos\alpha \cos\beta \tag{18}$$

$$W_B = V \cos\beta \sin\alpha \tag{19}$$

$$V_B = V \sin\beta \tag{20}$$

Then the body-axis velocities are resolved to the inertial axes by the Euler angles as

$$\dot{H} = U_B \sin\theta - V_B \sin\phi \cos\theta - W_B \cos\phi \cos\theta \tag{21}$$

$$\dot{X} = U_B \cos\theta \cos\psi + V_B (\sin\phi \sin\theta \cos\psi - \cos\phi \sin\psi) + W_B (\cos\phi \sin\theta \cos\psi + \sin\phi \sin\psi) \tag{22}$$

$$\dot{Y} = U_B \cos\theta \sin\psi + V_B (\sin\phi \sin\theta \sin\psi + \cos\phi \cos\psi) + W_B (\cos\phi \sin\theta \sin\psi - \sin\phi \cos\psi) \tag{23}$$

The dynamic pressure equation is

$$\bar{Q} = \frac{1}{2} \rho V^2 \tag{24}$$

where the density (ρ) is a direct table look-up.

The rotational equations of motion are written in the body axis system.

The pitch equation is

$$\dot{Q} = \frac{\Sigma M}{I_{yy}} + \frac{I_{xz}}{I_{yy}} (R^2 - P^2) - \frac{(I_{zz} - I_{xx})}{I_{yy}} P R \tag{25}$$

The roll equation is

$$\dot{P} = \frac{\Sigma L}{I_{xx}} + \frac{I_{xz}}{I_{xx}} \dot{R} - \frac{(I_{zz} - I_{yy})}{I_{xx}} QR + \frac{I_{xz}}{I_{xx}} PQ \tag{26}$$

The yaw equation is

$$\dot{R} = \frac{\Sigma N}{I_{zz}} + \frac{I_{xz}}{I_{zz}} \dot{P} - \frac{(I_{yy} - I_{xx})}{I_{zz}} PQ - \frac{I_{xz}}{I_{zz}} QR \tag{27}$$

The body rates are used to compute the Euler angles by the equations

$$\dot{\theta} = Q \cos \phi - R \sin \phi \tag{28}$$

$$\dot{\phi} = P + \dot{\psi} \sin \theta \tag{29}$$

$$\dot{\psi} = \frac{(R \cos \phi + Q \sin \phi)}{\cos \theta} \tag{30}$$

Control of the spacecraft is accomplished by the deflection of elevons and rudder. Roll control is achieved by differentially deflecting the elevons. The roll controller (ailerons) is computed by

$$\delta_a = \delta_{e_{left}} - \delta_{e_{right}} \tag{31}$$

The total surface deflections are

$$\delta_e = \delta_{e_P} + K_Q Q \tag{32}$$

$$\delta_r = \delta_{r_P} + K_R R + K_{\delta_a} \delta_a \tag{33}$$

$$\delta_a = \delta_{a_P} + K_p P \tag{34}$$

The limits placed on the surface deflections are

$$|\delta_e| \leq 25° \tag{35}$$

$$|\delta_a| \leq 10° \tag{36}$$

$$|\delta_r| \leq 25° \tag{37}$$

The moment equations are

$$\Sigma L = C_\ell \bar{Q} S b \tag{38}$$

$$\Sigma M = C_m \bar{Q} S \ell \tag{39}$$

$$\Sigma N = C_n \bar{Q} S b \tag{40}$$

The expansion for C_ℓ, C_m, and C_n is in Equations 3, 5, and 6.

A hybrid simulation of the spacecraft concept was programmed using the equations and data discussed in Section 3 and the above equations. The hybrid simulation provides a computational tool for application that lies somewhere between a pure digital and a pure analog simulation. The digital computer portion of the hybrid computer provided a function generator and storage device for all of the detailed aerodynamic data.

Equations 7 through 24 were programmed on the digital computer in Fortran II. These equations were numerically integrated and the integration scheme included terms to compensate for phase-lag due to the sampling time. The overall digital computer cycle time was 0.06 second, which not only included the solution to the indicated differential equations but also the generation of the aerodynamic data for the analog computer.

Equations 25 through 40 were programmed on the analog computer. The analog computer was the device used to link the visual display and the cockpit to the overall simulation. Approximately three-quarters of the available equipment on a Comcor CI-5000 analog computer was used.

SECTION 5

RESULTS

5.1 OVERALL TRAJECTORIES

Trajectories were flown on the simulator starting at an altitude of 100,000 feet and initial Mach numbers of 3.5, 4, and 5. The piloting task was to fly a given flight path angle profile. The profiles consisted of a constant flight path angle to wing deployment and then transition to a new flight path angle which was held to landing site acquisition. Figure 5-1 presents spacial histories for the various simulated flights. All of the flights were flown with the stability augmentation system that is discussed later in this section.

With an initial Mach number of 5 at 100,000 feet, this spacecraft is capable of flying constant flight paths of from 5 to 7 degrees. At flight paths below 5 degrees, the velocity dropoff was too large and the trim angle of attack required was beyond the trim capability of the vehicle control system. For flight path angles greater than 7 degrees, the speed dropoff is not great enough and therefore the vehicle's velocity between 45,000 and 35,000 feet was well above the transonic value desired for starting wing deployment. The flight path range for an initial Mach number of 4 was 5 to 8 degrees; for an initial Mach number of 3.5 it was 7 to 10 degrees.

Figures 5-2 through 5-4 present the time histories of various parameters for flight with initial Mach numbers of 5, 4, and 3, respectively. Summaries of the trim angle of attack and elevator requirements for the range of altitudes and velocities of interest are presented in Figures 5-5 through 5-10.

5.2 WING DEPLOYMENT

Since this spacecraft concept employs a switch-blade wing it is felt that partial wing deployment can occur at transonic speeds. However, the wing deployment should occur at an altitude and distance from the landing site sufficient enough to allow small cross-range and down-range errors to be nulled out by the high maneuverability allowed with increased L/D due to wing deployment. Results of the present study indicate that for the switch-blade wing concept, the best speed for start of wing deployment is at a Mach number of approximately 0.95.

At this Mach number aeroelastic effects are minimum and, therefore, flutter and wing divergent problems are circumvented. This Mach number occurs between 45,000 and 35,000 feet in altitude for the flight path profiles presented earlier. This speed and altitude allows sufficient time and maneuvering capability for landing site acquisition.

In this range of altitude, maximum down range attainable is about 325,000 feet, or about 60 miles.

During wing deployment, the vehicle experiences a heaving motion and increase in angle of attack due to an increase in the overall lift coefficient. To reduce the lift, the pilot does a push-over maneuver. The piloting objective during wing deployment is to maintain a constant flight path angle. Figure 5-11 presents the wing deployment sequence for the pilot performing a push-over maneuver. The wing was swept at 1 deg/sec.

Without a push-over maneuver, the sink rate would reduce to zero and the vehicle would begin to climb due to the increase in lift. As the vehicle climbs, the velocity drops off in the exchange of kinetic energy for potential energy. The flight path oscillation, being only lightly damped, persists for several minutes. If the oscillation were uncontrolled it would be intolerable to the spacecraft crew. Reference 2 presents a detailed description of this maneuver.

If the deployment rates are greater than 1 deg/sec then the initiation Mach number must be less than 0.95. As an example, for a deployment rate of 2 deg/sec the initiation Mach number is 0.88 if the wing is to be fully deployed at Mach 0.65 or lower. A deployment rate of 0.5 deg/sec is also adequate and allows the pilot more time to perform the pitch-over maneuver. As the vehicle is presently configured there appears to be no need to deploy the wing at any speeds above Mach 0.95. Two reasons exist for partial deployment (to 75°) at supersonic speed. Partial deployment produces increased directional stability by increasing C_{n_β}. In addition, partial deployment reduces the high angle of attack pitch-up instability. With the wing designed for subsonic loads at 15° of sweep, it is felt that a flutter problem would not exist supersonically for partial deployment.

5.3 LANDING CHARACTERISTICS

The landing characteristics of this spacecraft concept were analyzed by flying piloted simulated landings with the hybrid computer and visual display. A time history of a landing without flaps is presented in Figure 5-12. An approach speed of 190 knots and 8-degree flight path angle was flown and a peak incremental load factor of 0.3g was reached during the flare. The landing speed is approximately 165 knots, and the flare initiation altitude is approximately 300 feet. At this speed, sufficient elevon deflection is available for roll control or additional pitch maneuvering. Figure 5-13 summarizes the landing characteristics by presenting flare load factor, flare initiation altitude and end of flare speeds versus approach speed for an 8-degree flight path angle. An 8-degree flight path angle was chosen because it is the approximate equilibrium glide angle of speeds of from 170 to 200 knots. Figure 5-14 presents the equilibrium glide angle versus speed.

5.4 HANDLING QUALITIES

5.4.1 LONGITUDINAL. The handling qualities of this spacecraft concept have been analyzed in terms of the existing military specification for flying quality of piloted airframes.

The most significant longitudinal specifications determine the short period response. The short period damping must range between 0.35 and 1.3. Figures 5-15 and 5-16 show that the unaugmented vehicle is unsatisfactory over most of the conditions. This is an expected characteristic, particularly in the supersonic regime. A simple solution is a pitch rate damper which feeds into the elevator a signal proportional to pitch rate. Figure 5-16 also shows the effects of feeding back pitch rate with a gain of 1 deg/(deg/sec). As can be seen in this figure, the gain is insufficient at altitudes above 75,000 feet with wing stowed. Satisfactory damping of about 0.6 to 0.9 can be obtained above 75,000 feet by doubling the gain to 2 deg/(deg/sec).

The short period frequency requirement is related to the ratio $\omega_{n_{sp}}^2/(n_z/\alpha)$, where $\omega_{n_{sp}}$ is the short period frequency and (n_z/α) is the steady state normal acceleration per radian of angle of attack. It can be shown that initial pitch acceleration to steady state normal acceleration is proportional to $\omega_{n_{sp}}^2/(n_z/\alpha)$ and that the numerator zero in the pitch transfer function is also proportional to $\omega_{n_{sp}}^2/(n_z/\alpha)$. Figure 5-17 shows that this vehicle meets the $\omega_{n_{sp}}^2/(n_z/\alpha)$ specification. The pitch damper increases short period frequency improving the frequency characteristic further.

The phugoid characteristics are satisfactory. The requirement is for a damping ratio of at least 0.04. Since phugoid damping is approximately equal to 1/(L/D), low L/D vehicles (such as this concept with wing retracted) tend to have satisfactory phugoid characteristics. The pitch damper improves the phugoid damping.

5.4.2 LATERAL-DIRECTIONAL. The bare airframe has many undesirable hypersonic characteristics. The large dihedral effect coupled with low directional stability and low roll damping results in a coupled roll-spiral mode above Mach 2. This condition is characterized by a low frequency oscillation in roll rate with a zero steady state value. The condition is not permitted by the military specification. (The situation is further aggravated by the cross-over in sign of yaw due to aileron above $M \approx 3.0$, as illustrated in Figure 3-20.) The negative yaw moment at Mach numbers greater than 2.5 makes it difficult to generate independent roll and yaw moments, making compensation difficult. As an example, at M = 3.5 and H = 100,000 ft:

$$L_{\delta a} = +2.3398/\text{sec}^2$$
$$N_{\delta a} = -0.282350/\text{sec}^2$$
$$N_{\delta r} = -0.17354/\text{sec}^2$$

$$L_{\delta r} = 1.0468/sec^2$$

or

$$\frac{N_{\delta a}}{L_{\delta a}} = -0.121$$

$$\frac{N_{\delta r}}{L_{\delta r}} = -0.166$$

Figure 5-18 illustrates Dutch roll characteristics. The ϕ/V_e ratio is plotted in Figure 5-19. The excessive roll due to sideslip is indicative of roll reversal. Figure 5-20a illustrates a typical response with a coupled roll-spiral mode. The stability augmentation is extremely difficult, with considerable scheduling of gains needed. Figure 5-20b illustrates an augmented response. The Dutch roll frequency has been raised from 2.4 rad/sec to 7.8 rad/sec while the damping ratio went from 0.01 to 0.46. The roll mode time constant is still too long at 1.7 sec. (The requirement is a maximum of 1.4 seconds.) The compensation for this case is unacceptable at lower Mach numbers. The roll mode time constant could be reduced and the initial oscillation in roll rate eliminated by employing a compensation filter in the feedback path possessing complex zeros to reduce the Dutch roll component. Figure 5-21 illustrates a roll response at M = 0.21 at sea level and the compensated response. The ϕ/V_e ratio is plotted in Figure 5-19. The excessive roll due to sideslip is indicative of roll reversal.

Lateral handling qualities can be improved by dropping the horizontal tail dihedral. This would permit improvement in the roll mode by feeding roll rate into the differential elevator. A flight research vehicle built to this concept could have a variable dihedral tail to examine this problem.

SECTION 6

CONCLUSIONS

This study determined the flight characteristics of a variable geometry spacecraft with a hypersonic lift to drag ratio of about 2. The switch-blade type wings, similar to those on the F-111, provide improved subsonic performance. The results of the analysis have been presented in terms of time histories, landing characteristic parameters, existing military specifications, and proposed entry vehicle specifications. The following conclusions are drawn:

a. The vehicle with its center of gravity located at 60.1 percent of the body length was dynamically stable longitudinally in the form of simple rate feedback for all points in the flight envelope. As to be expected, artificial pitch damping is necessary for satisfactory response.

b. At Mach numbers above 2 the vehicle exhibits a coupled roll-spiral mode. The present military specification considers this unsatisfactory in a bare airframe. Since this condition results from the high location of the vertical and the short tail arm in yaw, it is unlikely that the vehicle could be simply corrected without augmentation.

c. The large dihedral angle in the horizontal tail reduces the coordinated roll effectiveness. During landing approach, maximum roll rate available with even 10 degrees of control is about 15 deg/sec. At Mach 3.5 the effectiveness is more like 7.5 deg/sec. The inability to produce independent moments with the rudder and differential elevator at Mach numbers above 3 means that augmentation is extremely difficult and sensitive to exact characteristics. Reduced tail dihedral is necessary at these Mach numbers to permit adequate augmentation.

d. Wing deployment begins transonically at Mach 0.95 and 35,000 ft. A deflection rate of 1 deg/sec is satisfactory and full deployment occurs by Mach 0.6 and 28,000 ft.

e. The vehicle has good landing characteristics. An approach speed of 190 knots at a flight path angle of 8 degrees was satisfactory. The flare was initiated at 300 feet of altitude. A conventional altitude rate flare computer was used with a peak incremental normal acceleration of 0.3g.

f. It is recommended that a vehicle of this type have a variable dihedral horizontal tail which would be programmed as a function of Mach number thereby minimizing roll-yaw coupling problems.

APPENDIX A

SMALL PERTURBATION EQUATIONS

Since most handling qualities requirements are specified in terms of modes, frequencies, and damping, it is important to have a method which can readily evaluate these parameters. A digital computer program was designed to proceed from a description of the vehicle in terms of its mass properties and aerodynamic characteristics to the various transfer function. The program trims the vehicle to one of four possible conditions: (1) maximum L/D, (2) maximum lift, (3) flight path angle, and (4) load factor.

From the trim condition, dimensionalized stability coefficients are computed by perturbing in sequence all of the independent variables and noting the resulting change in the forces and moments. The resulting perturbation quantities, which are normalized to units of angular and linear acceleration, are the first partial derivative terms of the Taylor's series expansion about the trim point.

Equations A-1 and A-2 are the linearized small perturbation equations of motion for the longitudinal and lateral modes of motion respectively. These equations are the conventional set used in aircraft analysis.

	U	W	Q/s	N_z		δ_e
Axial Force	$-X_u$ $+s$	$Q_o - X_w$	$g\cos\theta$ $+W_o s$	0		X_{δ_e}
Normal Force	$-Q_o - Z_u$	$-Z_w$ $+(1-Z_{\dot{w}})s$	$+g\sin\theta$ $-(U_o + Z_q)s$	0	=	Z_{δ_e}
Pitch Moment	$-M_u$	$-M_w$ $-M_{\dot{w}} s$	0 $-M_q s$ $+s^2$	0		M_{δ_e}
Normal Acceleration	Q_o	0 $-s$	$-g\sin\theta$ $+U_o s$	1.		0

(A-1)

	β	P/s	R/s	N_y	δ_α	δ_r
Lateral Force	$\dot{V}_o - Y_\beta$ Vs	$-g\cos\theta$ $-(W_o + Y_p)s$	$-g\sin\theta$ $+(U_o - Y_R)s$	0	Y_{δ_α}	Y_{δ_r}
Roll Moment	0 $-L_\beta$	0 $-(L_p + Q_o I_{xz}/I_{xx})s$ $+s^2$	0 $-[L_R - Q_o(I_{zz} - I_{yy})I_{xx}]s$ $-(I_{xz}/I_{xx})s^2$	0	L_{δ_α}	L_{δ_r}
Yaw Moment	0 $-N_\beta$	0 $-[N_p - Q_o(I_{yy} - I_{xx})/I_{zz}]s$ $-(I_{xz}/I_{zz})s^2$	0 $-[N_R - Q_o I_{xz}/I_{zz}]s$ $+s^2$	0	N_{δ_α}	N_{δ_r}
Lateral Acceleration	$-\dot{V}_o$ $-Vs$	$+g\cos\theta$ $W_o s$	$g\sin\theta$ $-U_o$	1.	0	0

=

(A-2)

REFERENCES

1. Spencer, Bernard, Jr., and Charles H. Fox., Jr., Hypersonic Aerodynamic Performance of Minimum Wave-Drag Bodies, NASA TR-R-250, 1966.

2. Kuchta, B. J., Flight Characteristics and Handling Qualities of Variable Geometry Spacecraft - Vol. 1 High L/D Concept with Single Pivot Two Position Skewed Wing, GDC-DDE68-003, Convair division of General Dynamics, 1969.

3. Flying Qualities of Piloted Aircraft, Military Specification MIL-F-8785B (ASG), 1969.

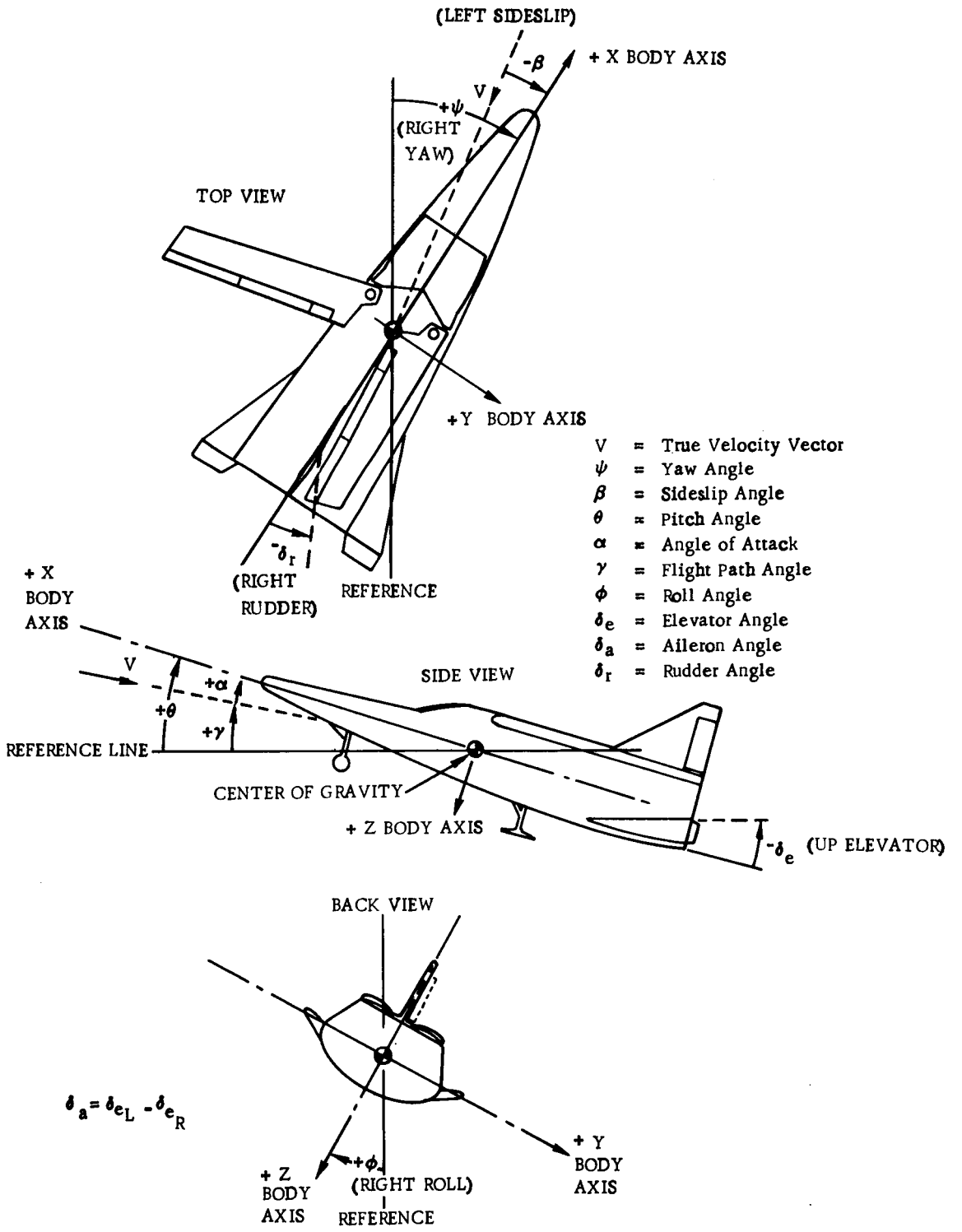

Figure 1-1. Sign Convention

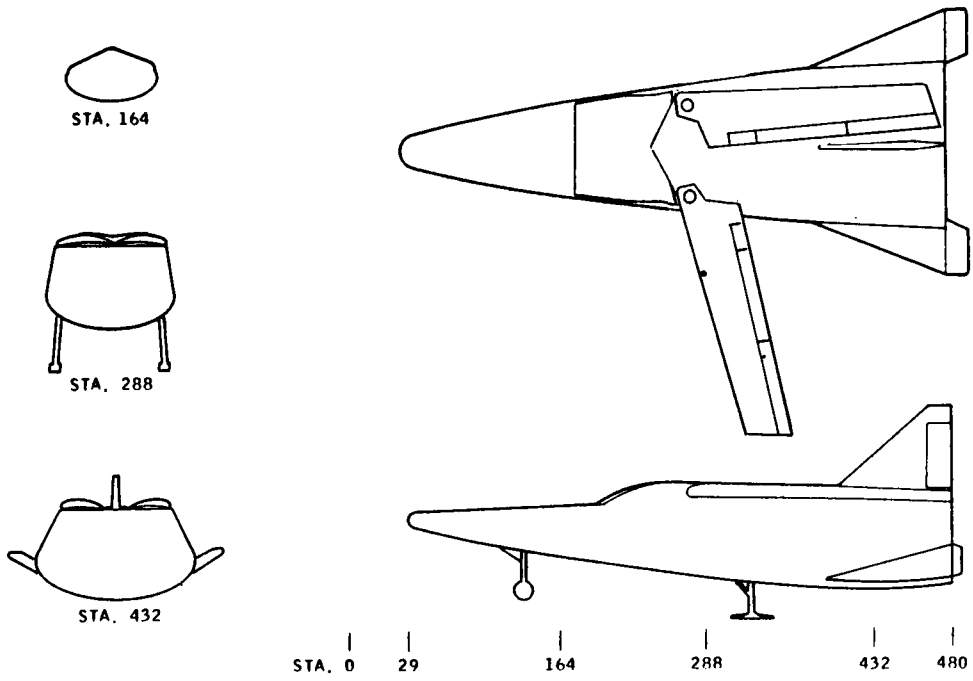

Figure 2-1. Drawings of the Hypersonic L/D ≈ 2 Vehicle

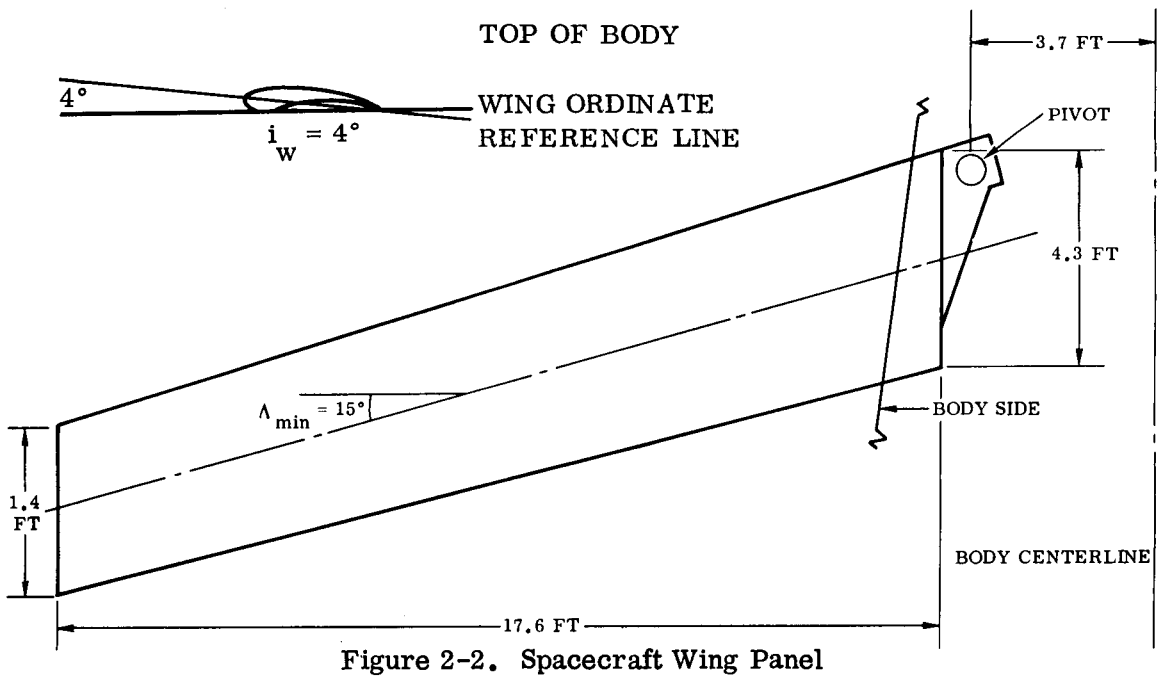

Figure 2-2. Spacecraft Wing Panel

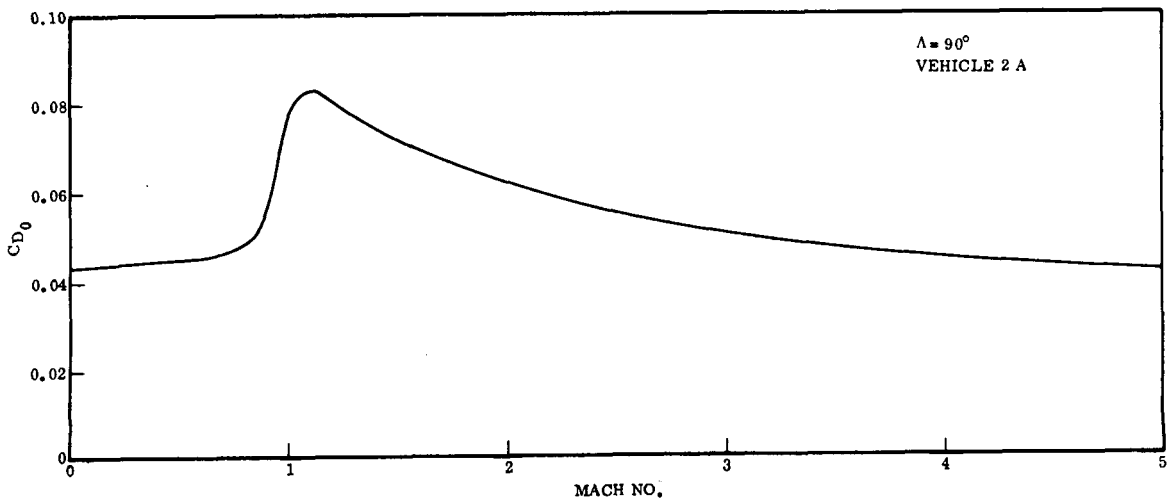

Figure 3-1. Drag Coefficient at Zero Angle of Attack

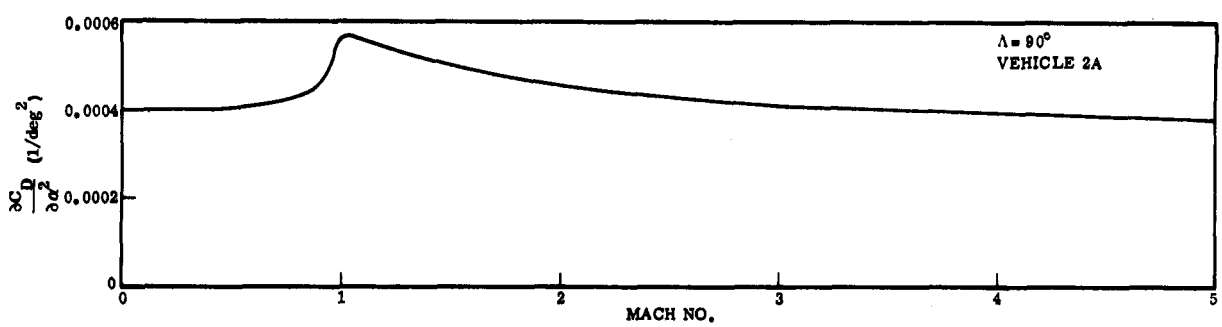

Figure 3-2. Partial Derivative of the Drag Coefficient With Angle of Attack Squared

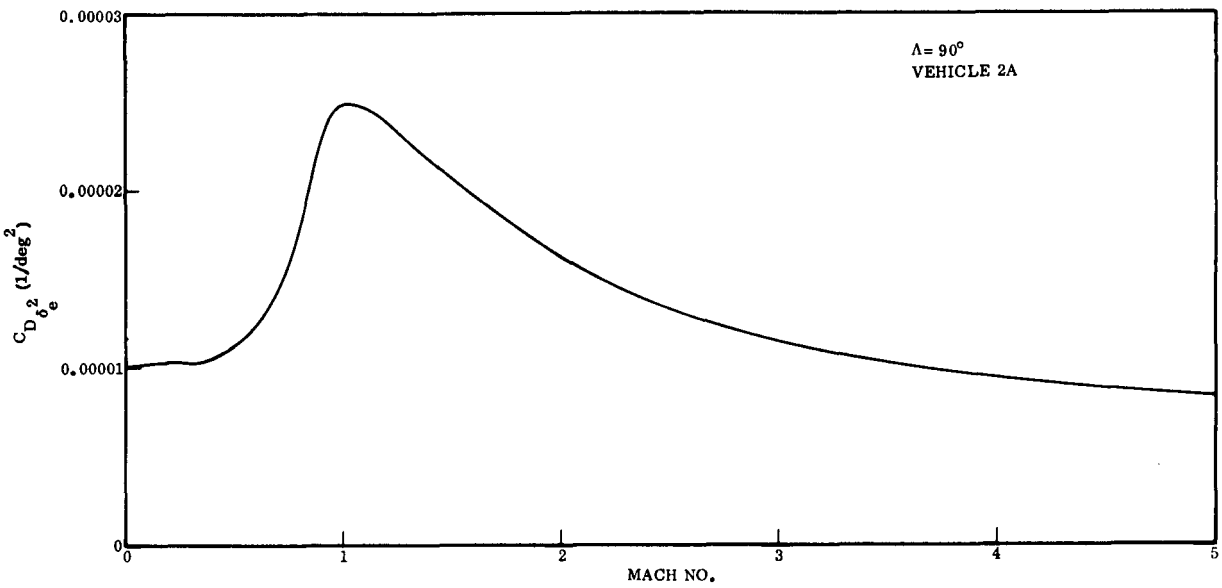

Figure 3-3. Partial Derivative of Drag Coefficient With Elevon Deflection Squared

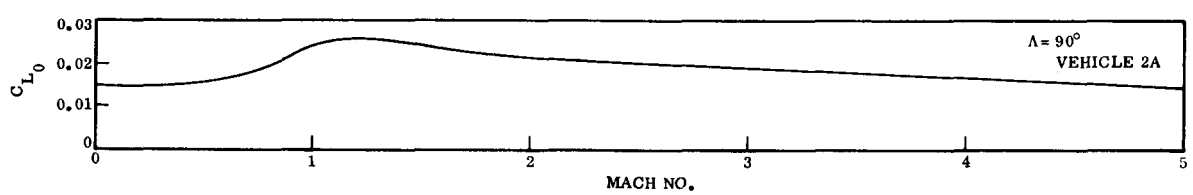

Figure 3-4. Lift Coefficient at Zero Angle of Attack

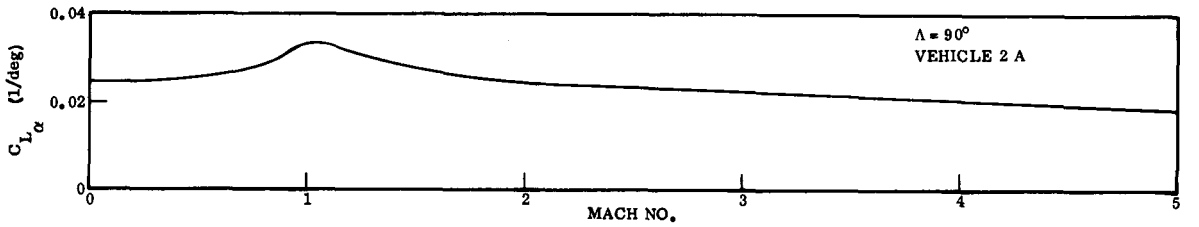

Figure 3-5. Lift Curve Slope

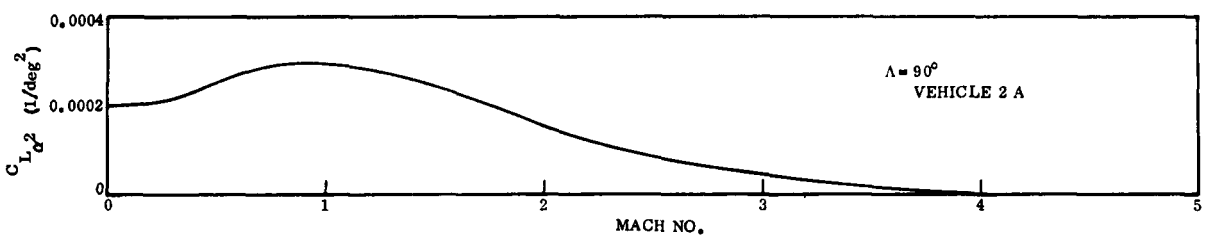

Figure 3-6. Partial Derivative of Lift Coefficient With Angle of Attack Squared

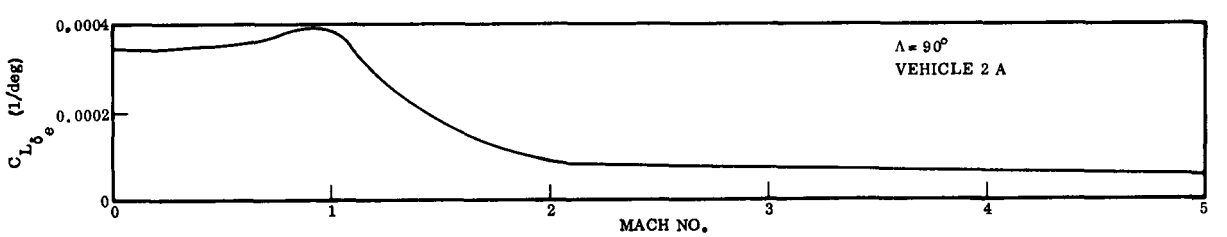

Figure 3-7. Partial Derivative of Lift Coefficient With Elevon Deflection ($|\delta_e| < 25°$)

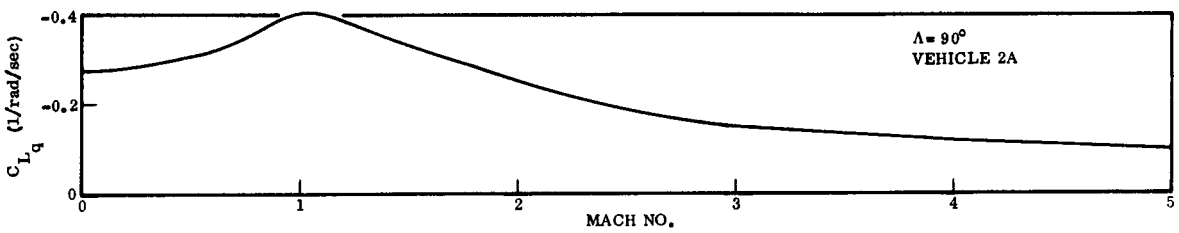

Figure 3-8. Lift Damping Derivative Due to Pitch Rate

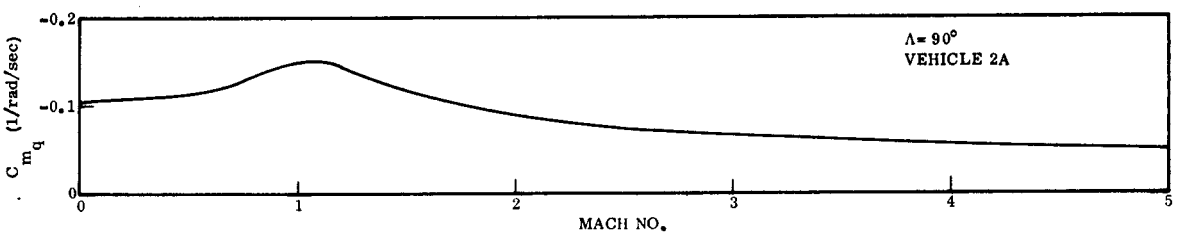

Figure 3-9. Pitch Moment Damping Derivative Due to Pitch Rate

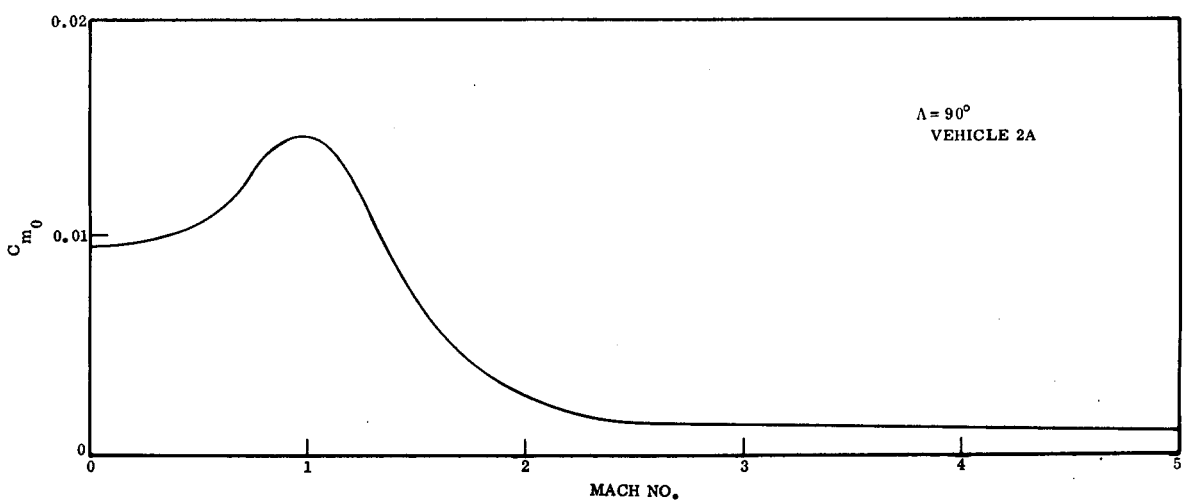

Figure 3-10. Pitch Moment Coefficient at Zero Angle of Attack

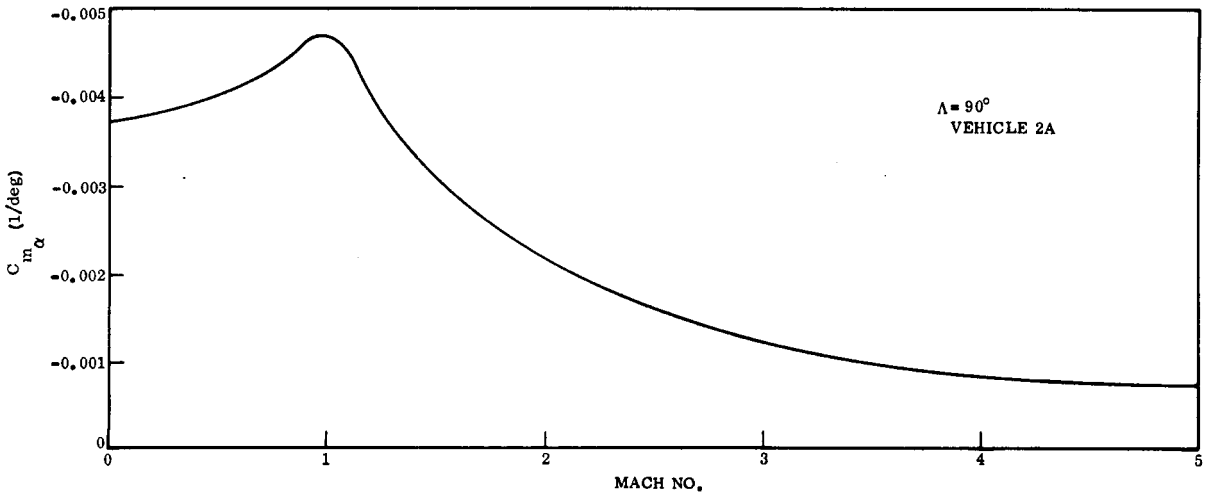

Figure 3-11. Partial Derivative of Pitch Moment Coefficient With Angle of Attack

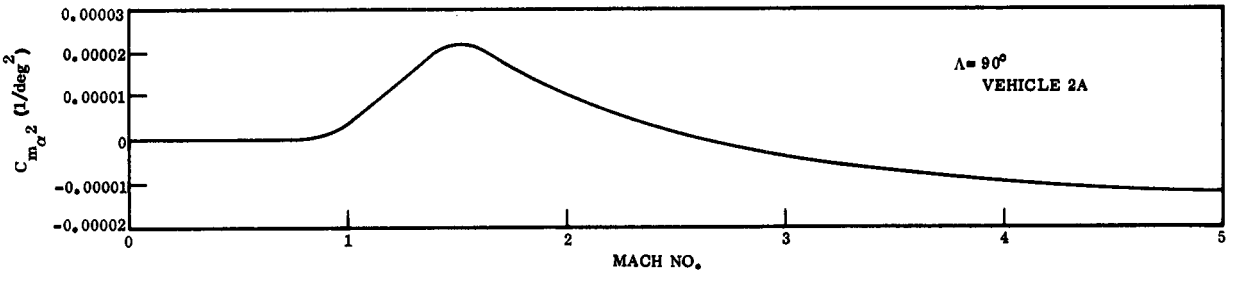

Figure 3-12. Partial Derivative of Pitch Moment Coefficient With Angle of Attack Squared

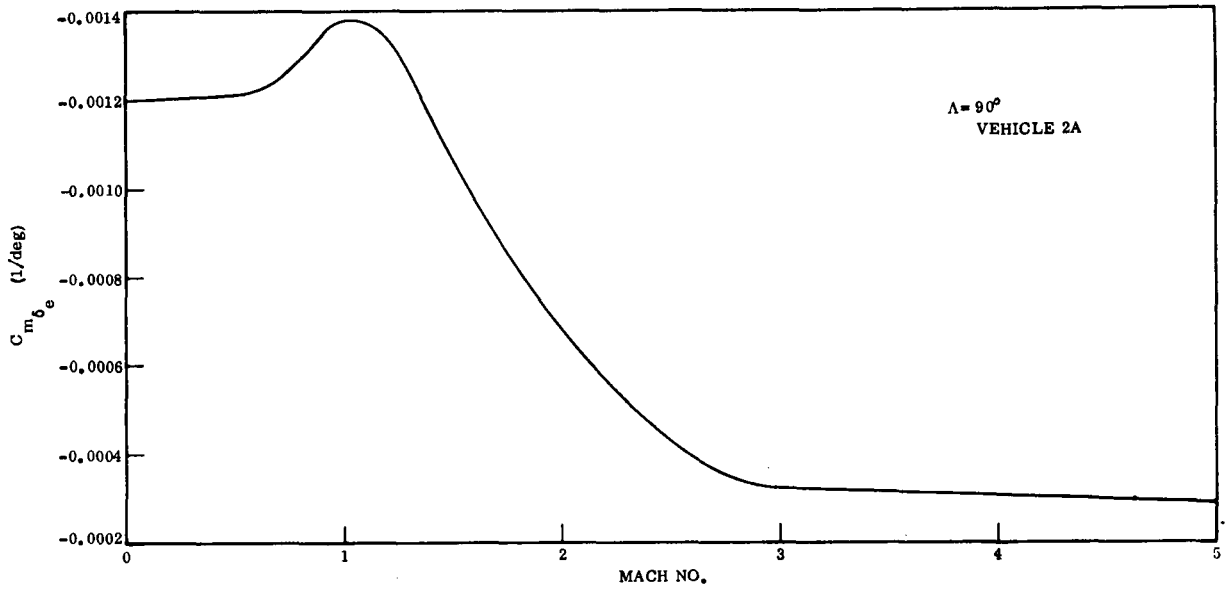

Figure 3-13. Partial Derivative of Pitch Moment Coefficient With Elevon Deflection ($|\delta_e| < 25°$)

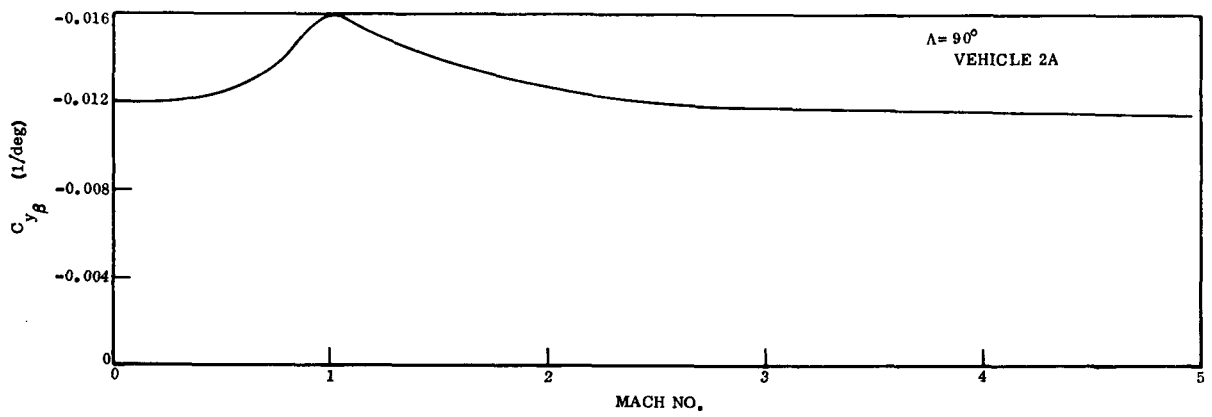

Figure 3-14. Side Force Stability Parameter

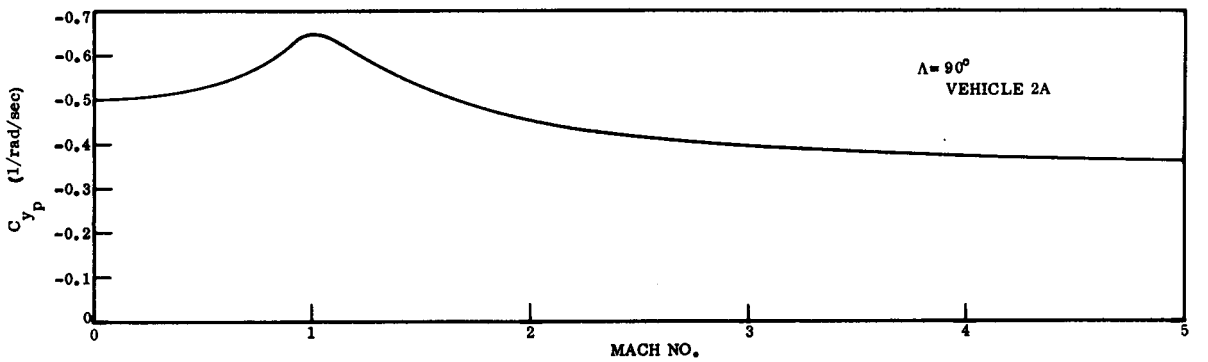

Figure 3-15. Partial Derivative of Side Force Coefficient With Roll Rate

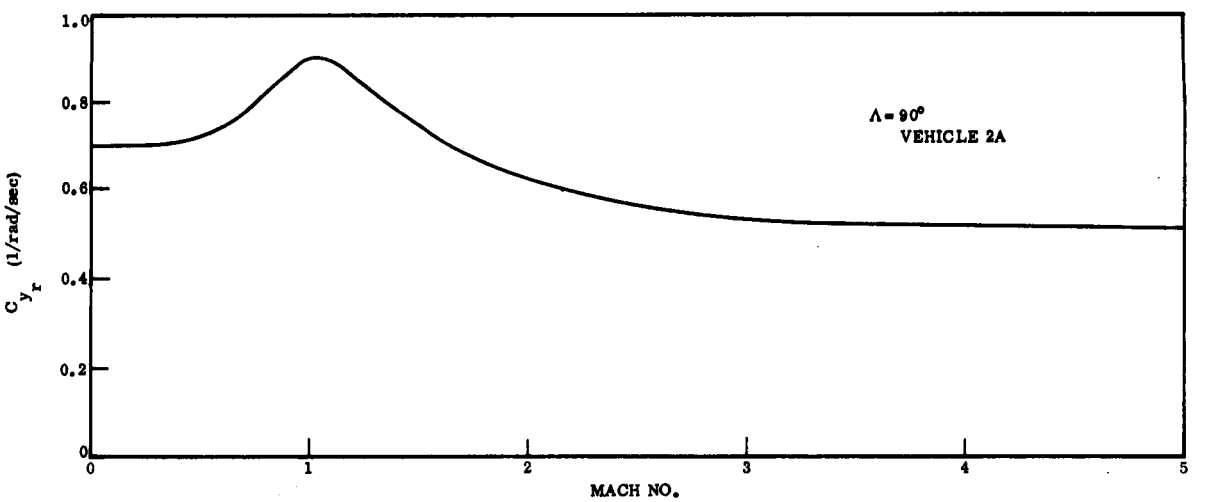

Figure 3-16. Partial Derivative of Side Force Coefficient With Yaw Rate

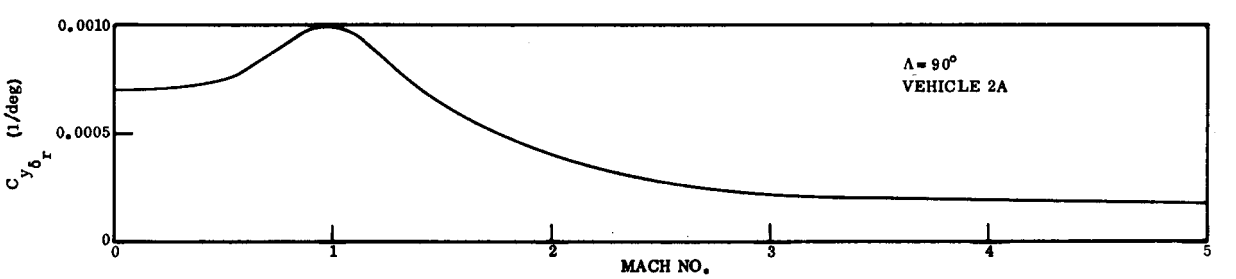

Figure 3-17. Partial Derivative of Side Force Coefficient With Rudder Deflection ($|\delta_r| < 25°$)

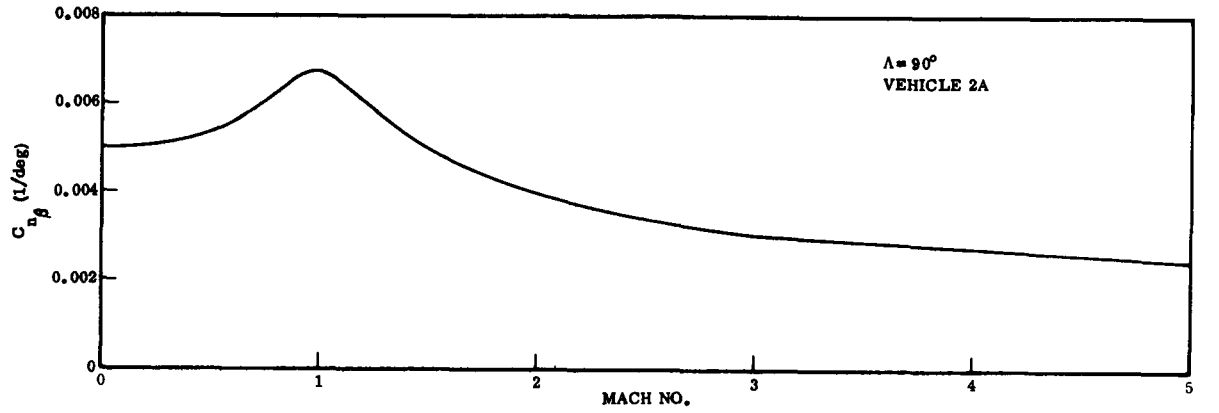

Figure 3-18. Directional Stability Coefficient

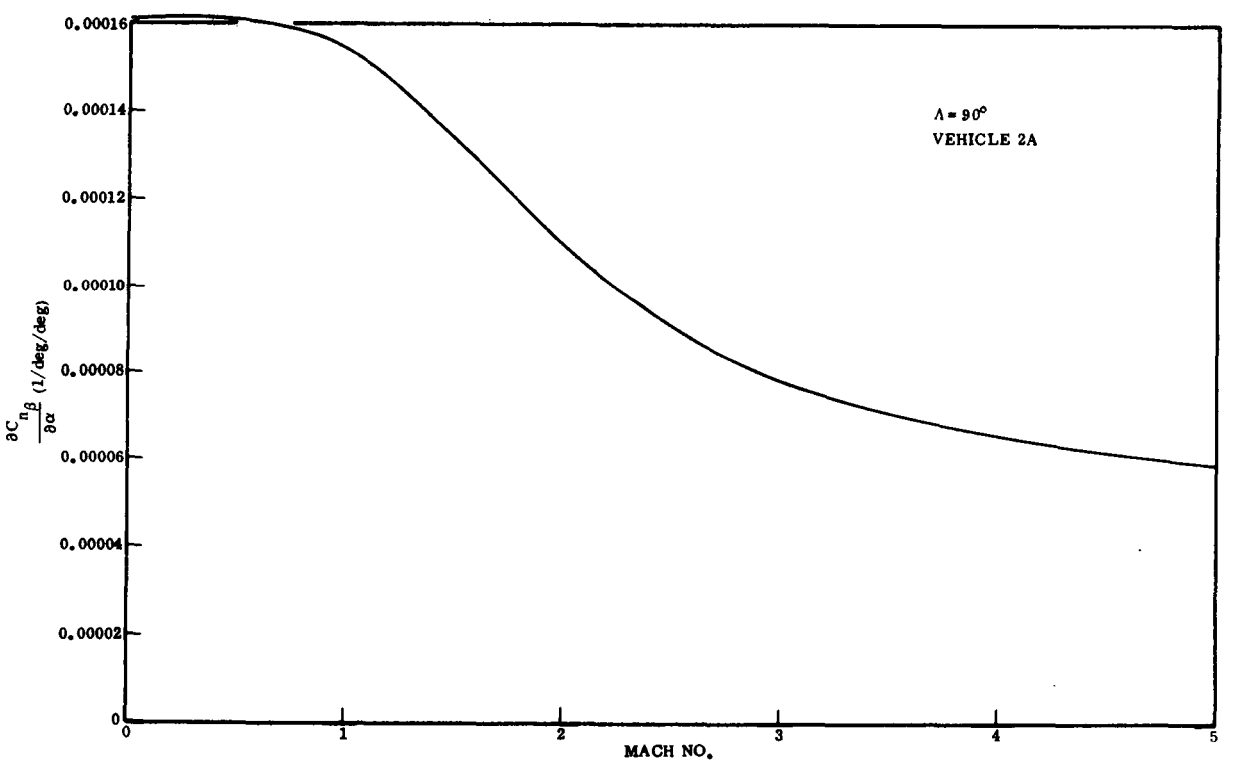

Figure 3-19. Partial Derivative of the Directional Stability Coefficient With Angle of Attack

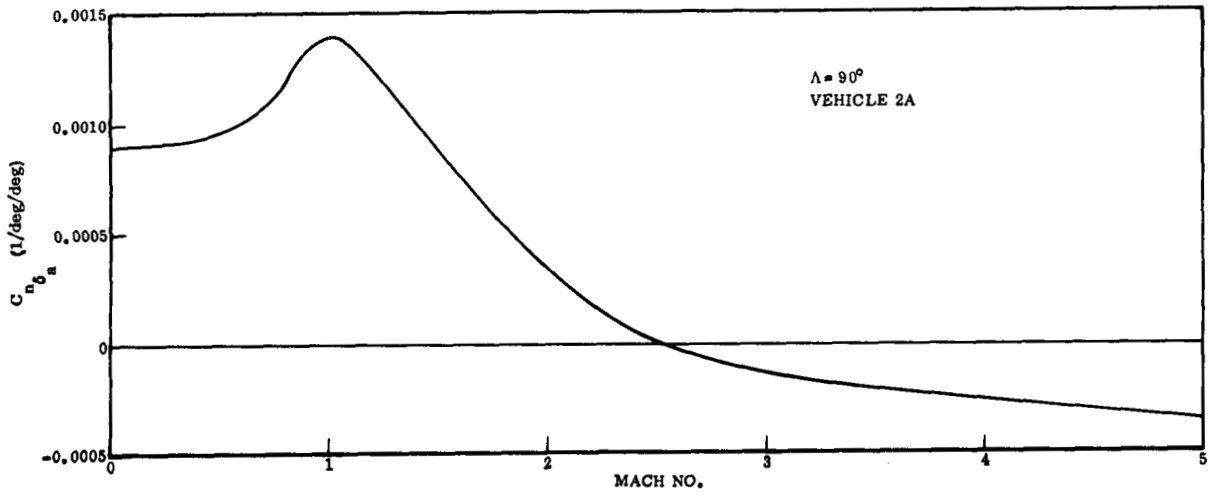

Figure 3-20. Yaw Moment Coefficient Due to Aileron Deflection ($|\delta_a| \leq 10°$)

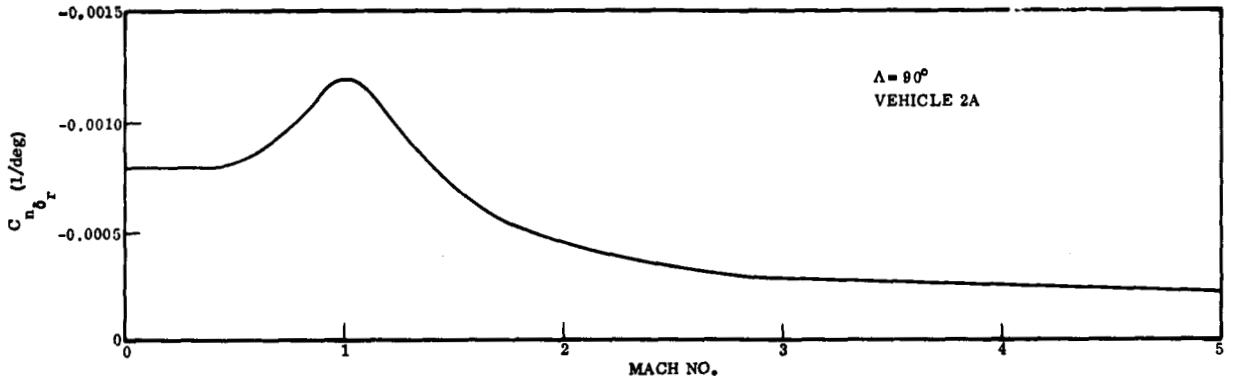

Figure 3-21. Yaw Moment Coefficient Due to Rudder Deflection ($|\delta_r| \leq 25°$)

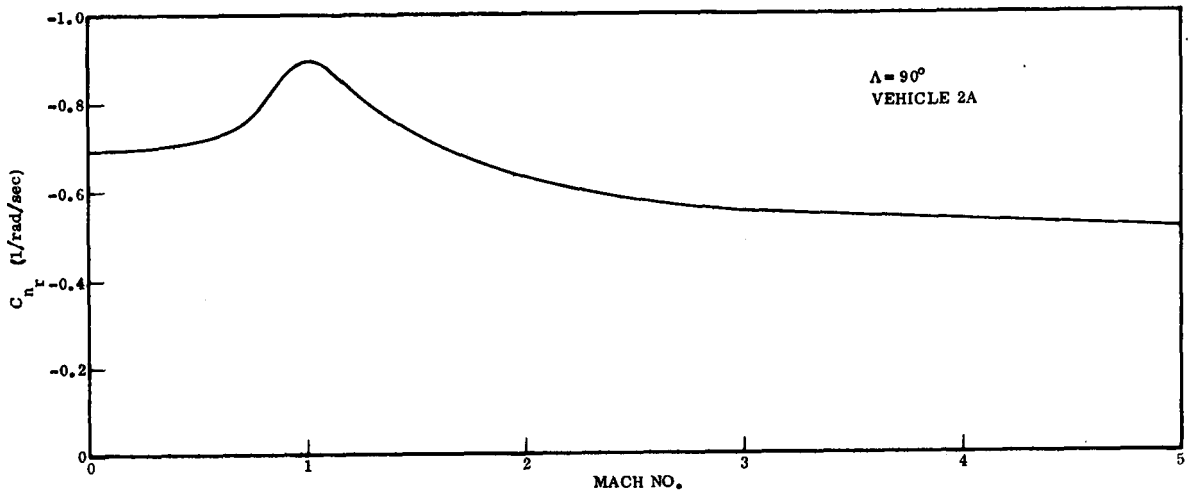

Figure 3-22. Yaw Moment Coefficient Due to Yaw Rate

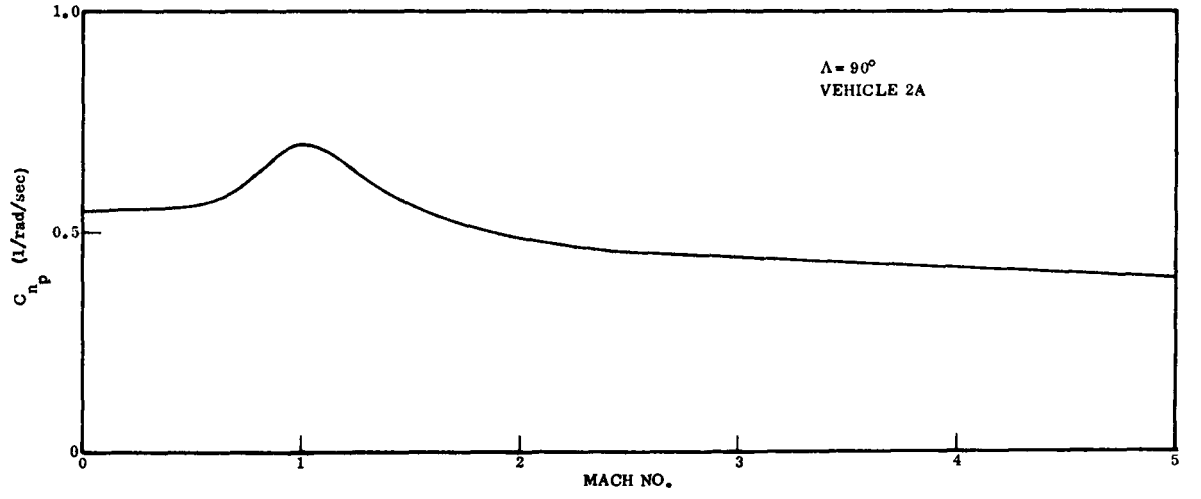

Figure 3-23. Yaw Moment Coefficient Due to Roll Rate

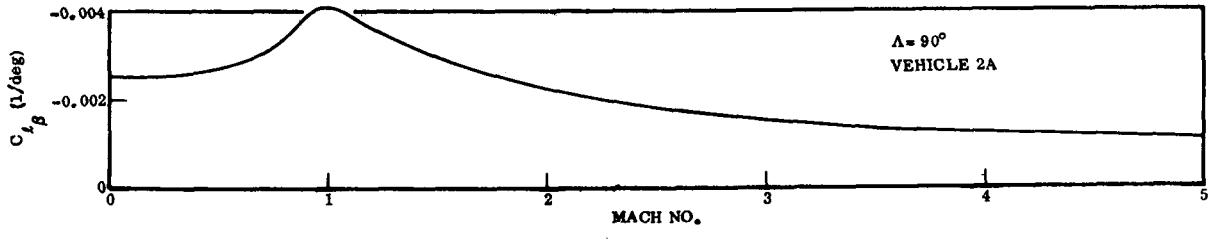

Figure 3-24. Roll Moment Coefficient Due to Sideslip

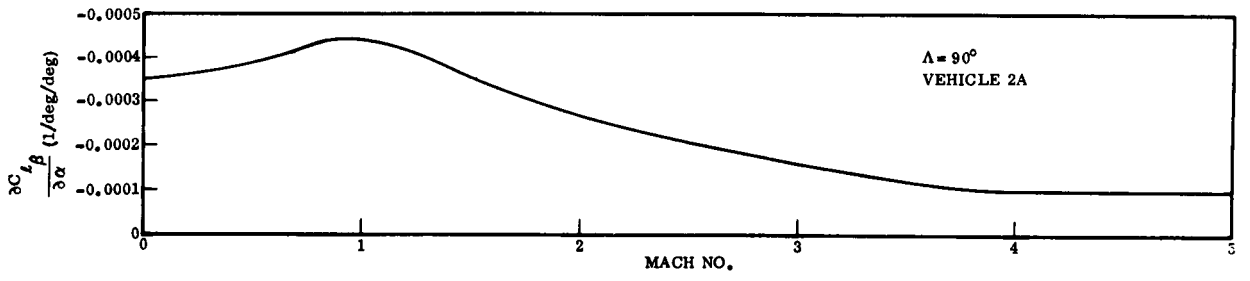

Figure 3-25. Partial Derivative of the Roll Moment Due to Sideslip Coefficient With Angle of Attack

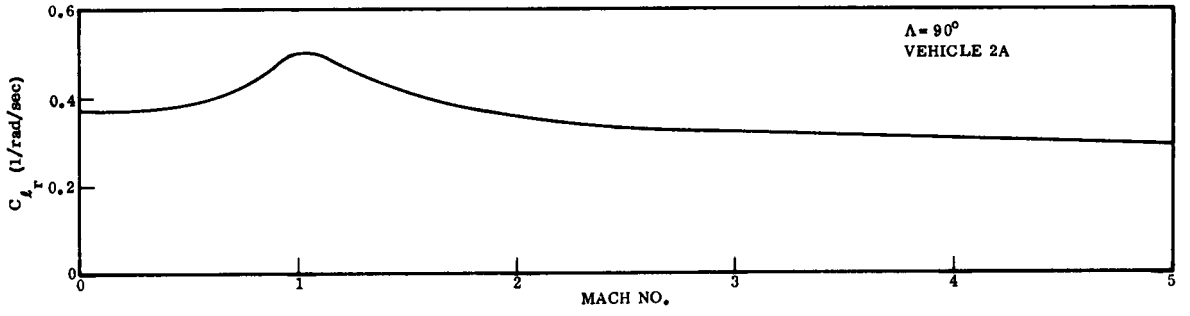

Figure 3-26. Roll Moment Coefficient Due to Yaw Rate

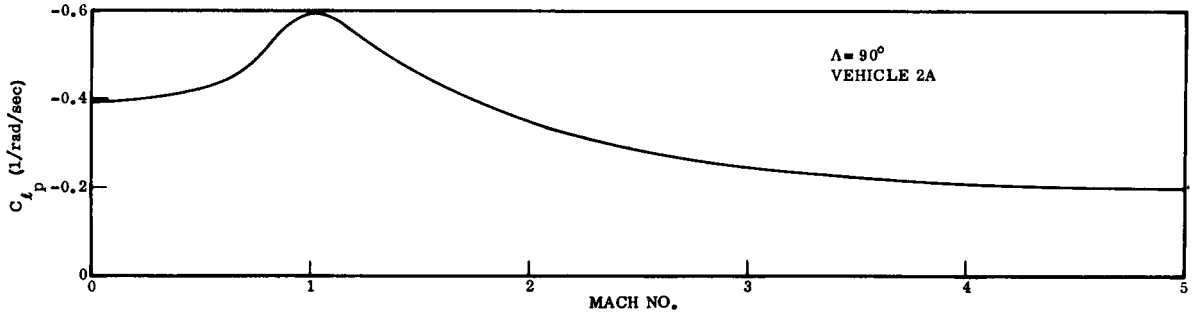

Figure 3-27. Roll Moment Coefficient Due to Roll Rate

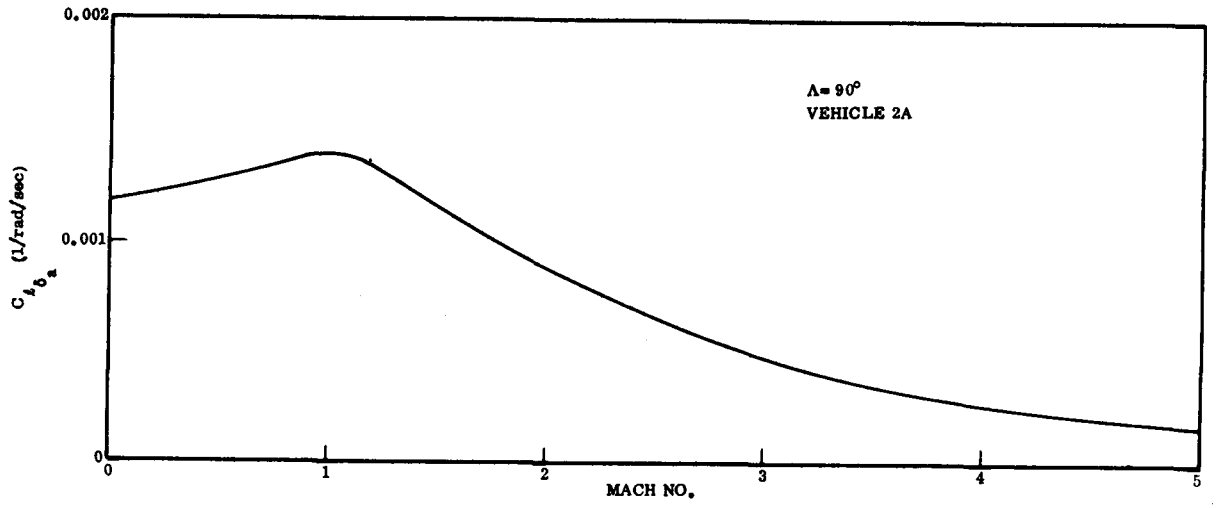

Figure 3-28. Roll Moment Coefficient Due to Aileron Deflection ($|\delta_a| \leq 10°$)

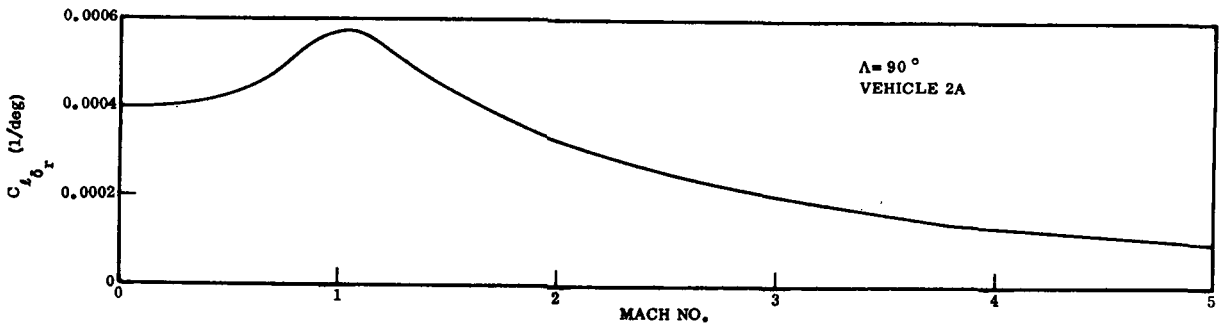

Figure 3-29. Roll Moment Coefficient Due to Rudder Deflection ($|\delta_r| < 25°$)

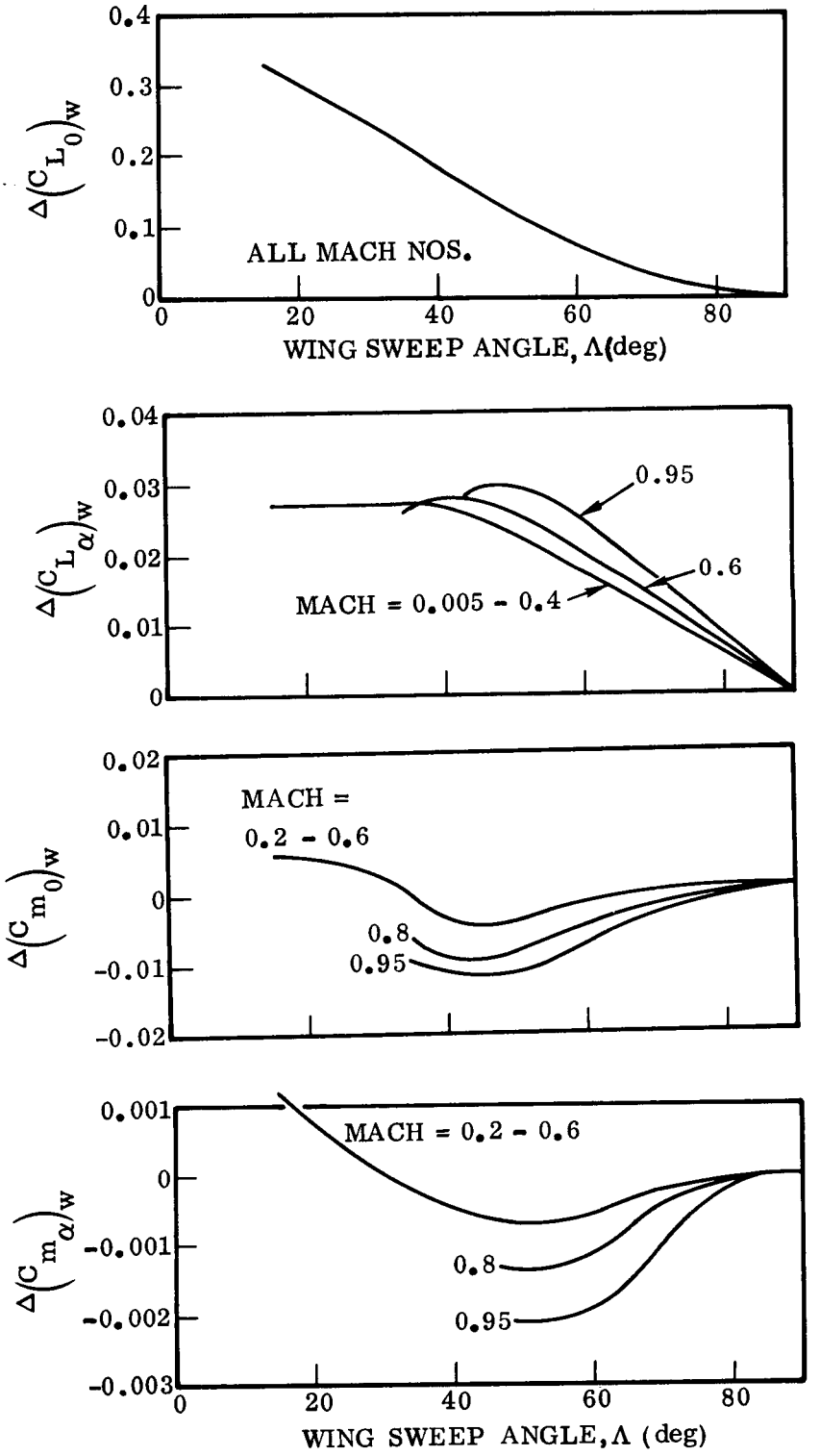

Figure 3-30. Wing Sweep Effects

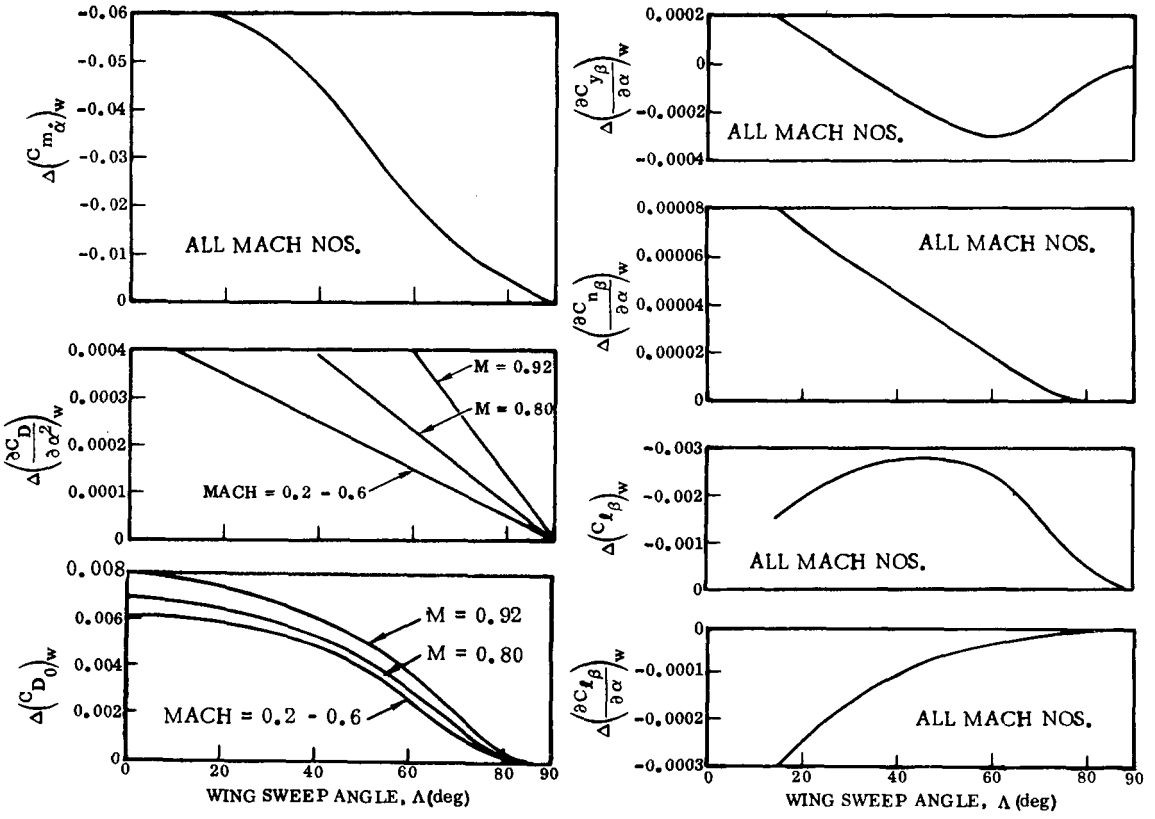

Figure 3-31. Wing Incremental Aerodynamics

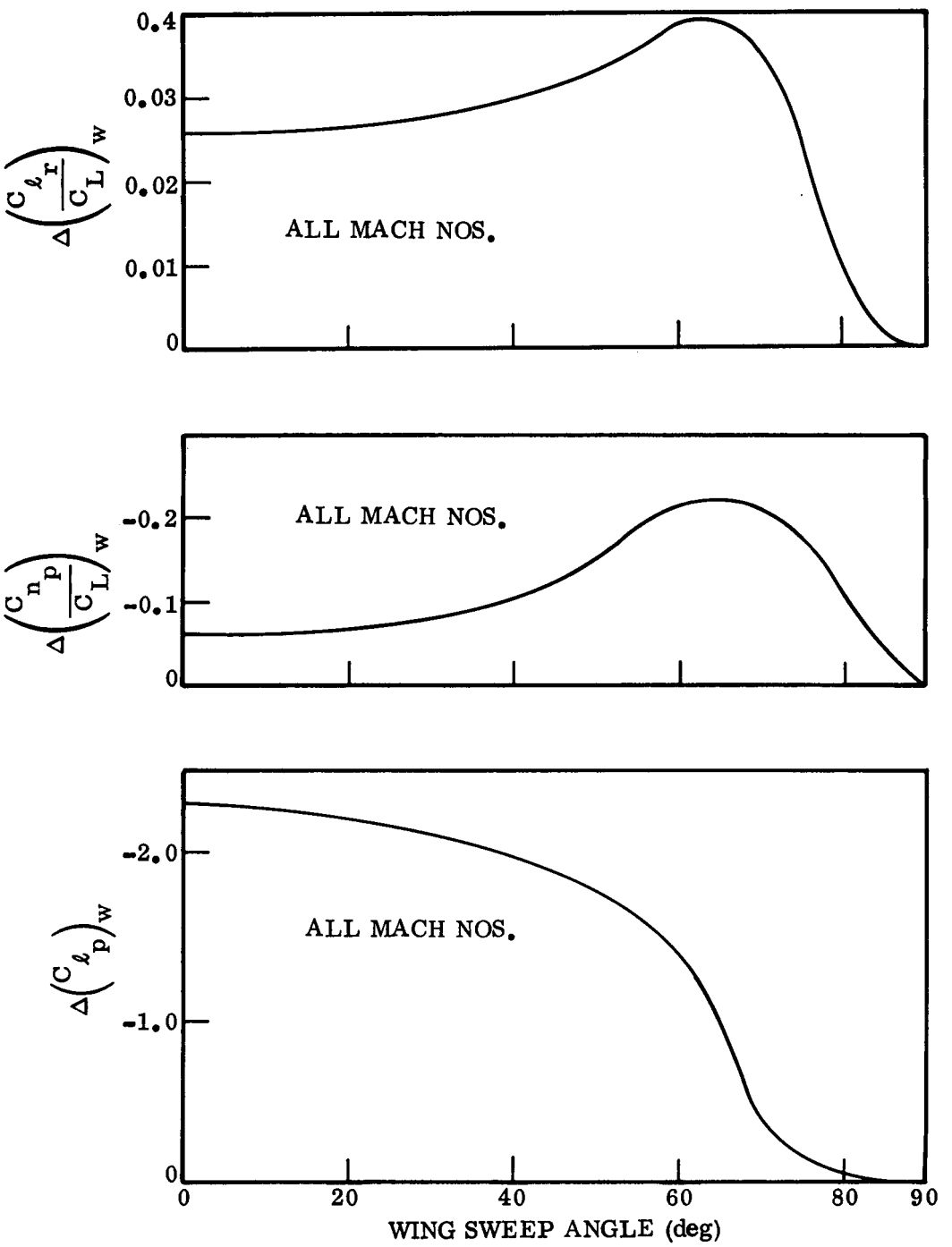

Figure 3-32. Subsonic Wing Incremental Lateral Aerodynamics

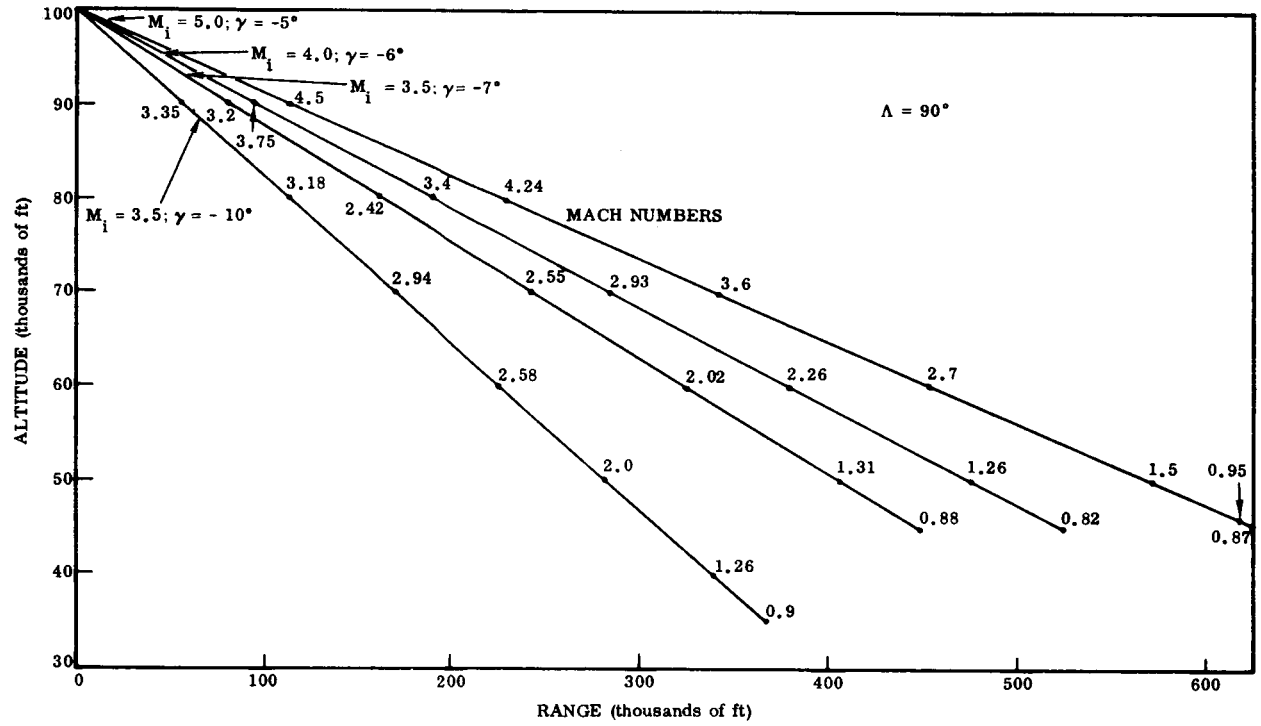

Figure 5-1. Spacial Histories of Simulated Flights

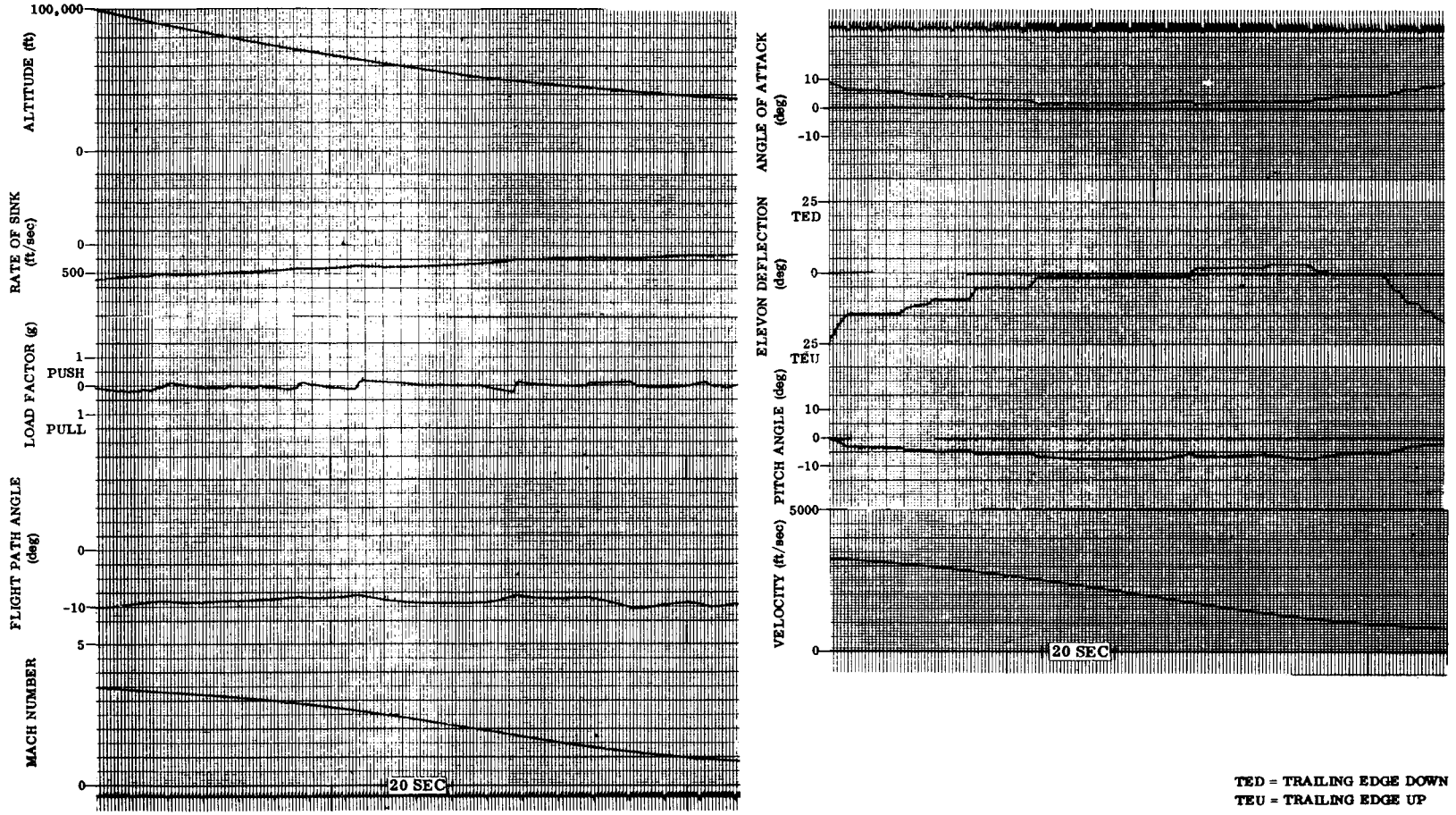

Figure 5-2. Time History; Trajectory $M_i = 3.5$, $\gamma = -10$ deg

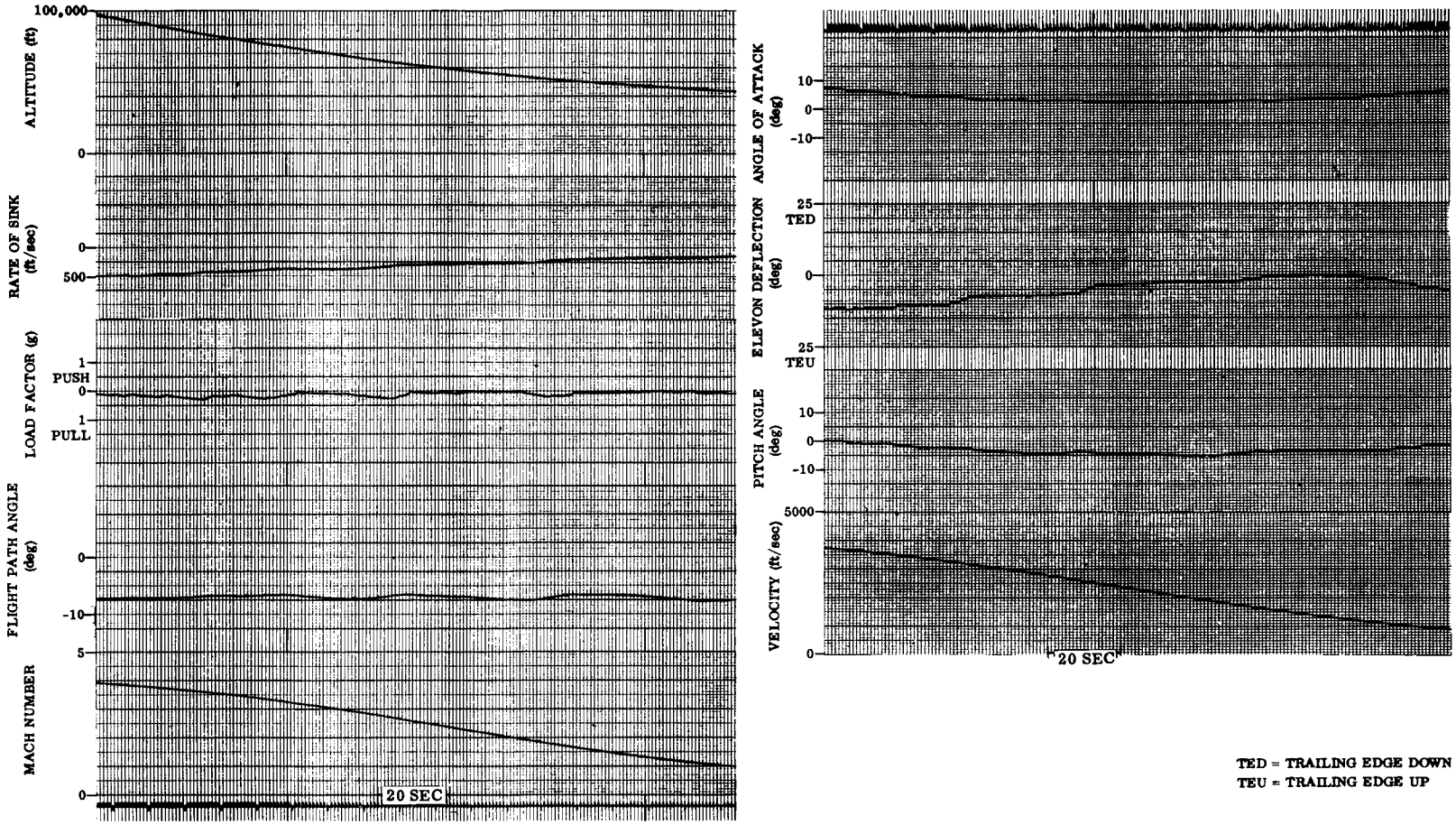

Figure 5-3. Time History; Trajectory $M_i = 4$, $\gamma = -7$ deg

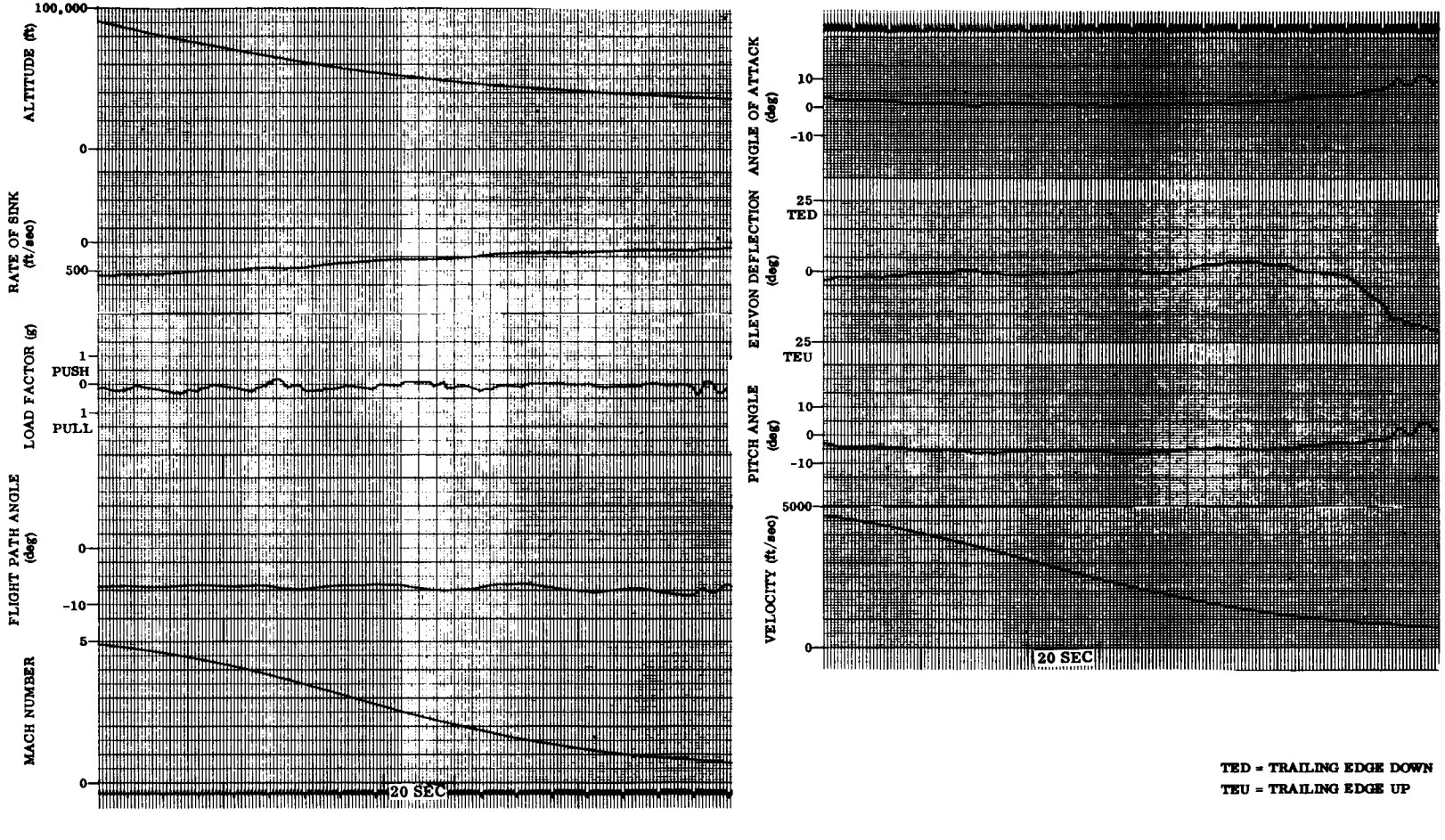

Figure 5-4. Time History; Trajectory $M_i = 5$, $\gamma = -7$ deg

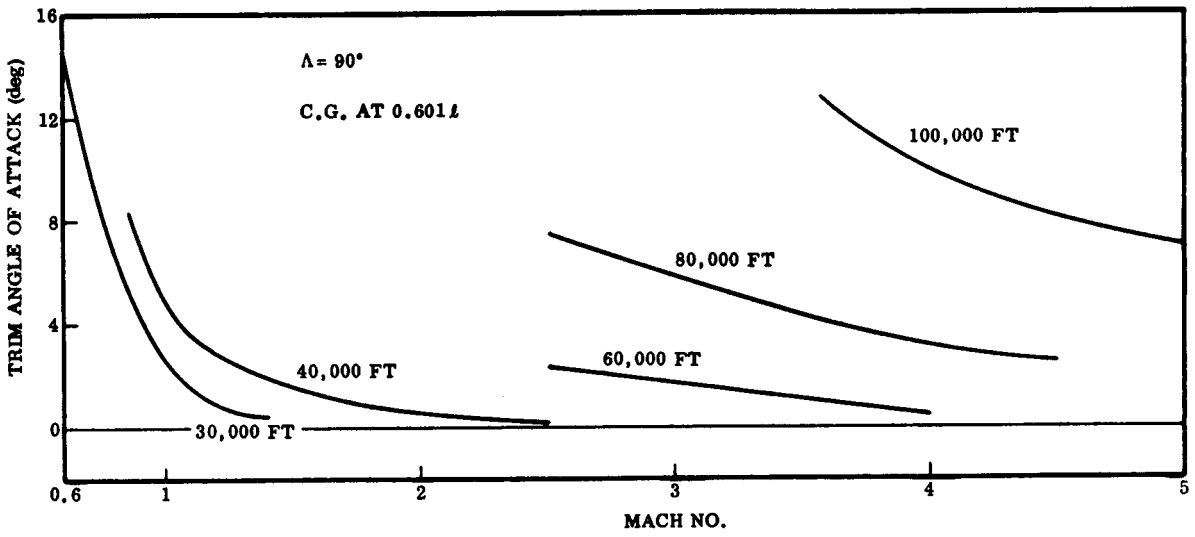

Figure 5-5. Trim Angle of Attack, $\Lambda = 90°$

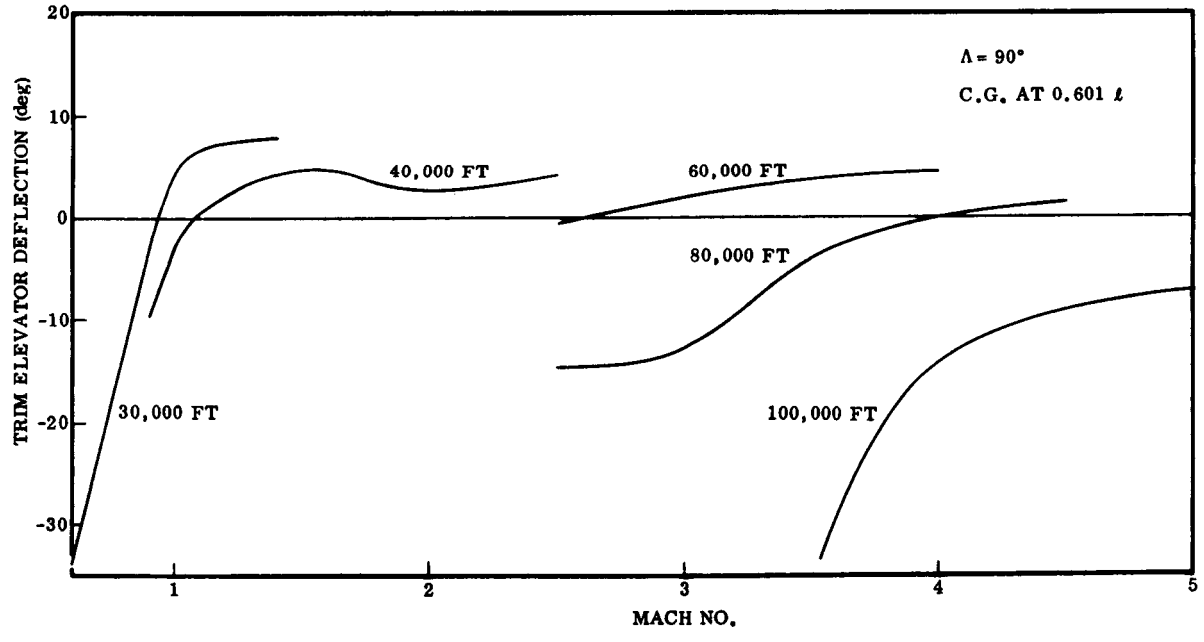

Figure 5-6. Trim Elevator Deflection, $\Lambda = 90°$

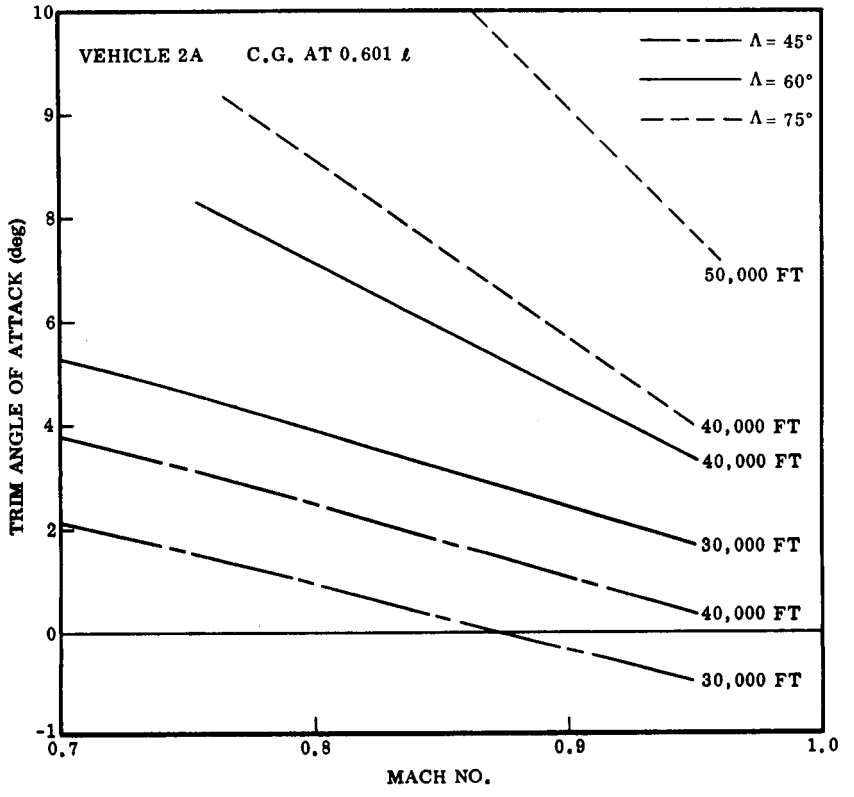

Figure 5-7. Trim Angle of Attack, Λ = 45°, 60°, 75°

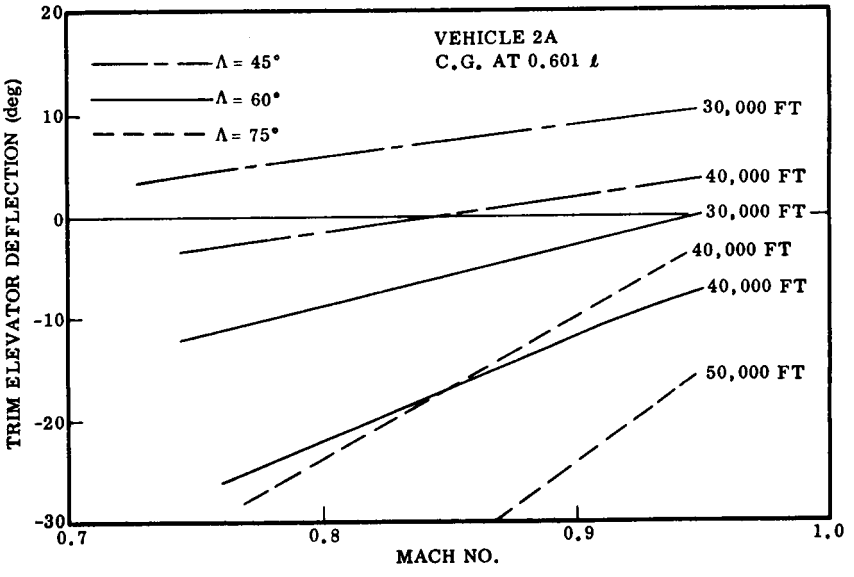

Figure 5-8. Trim Elevator Deflection, Λ=45°, 60°, 75°

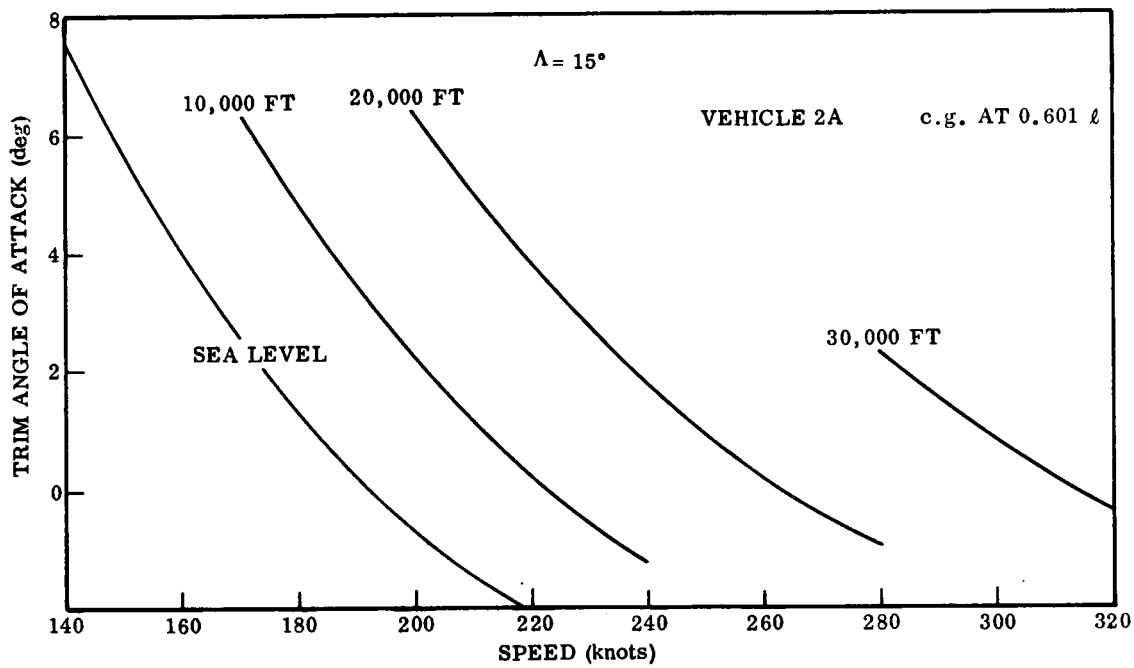

Figure 5-9. Trim Angle of Attack, Λ = 15°

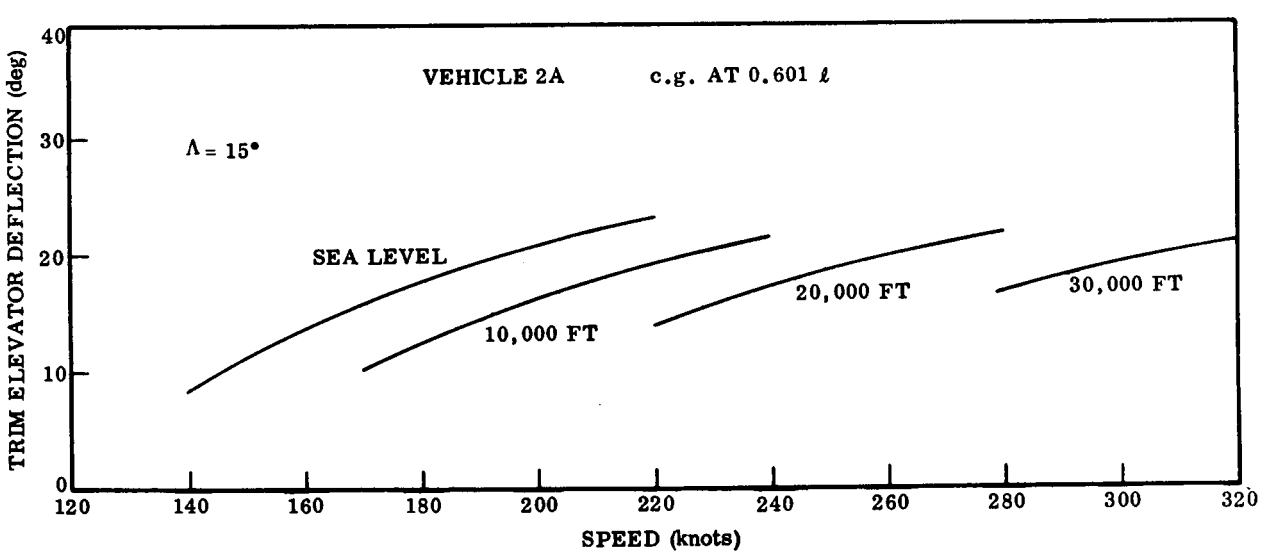

Figure 5-10. Trim Elevator Deflection, Λ = 15°

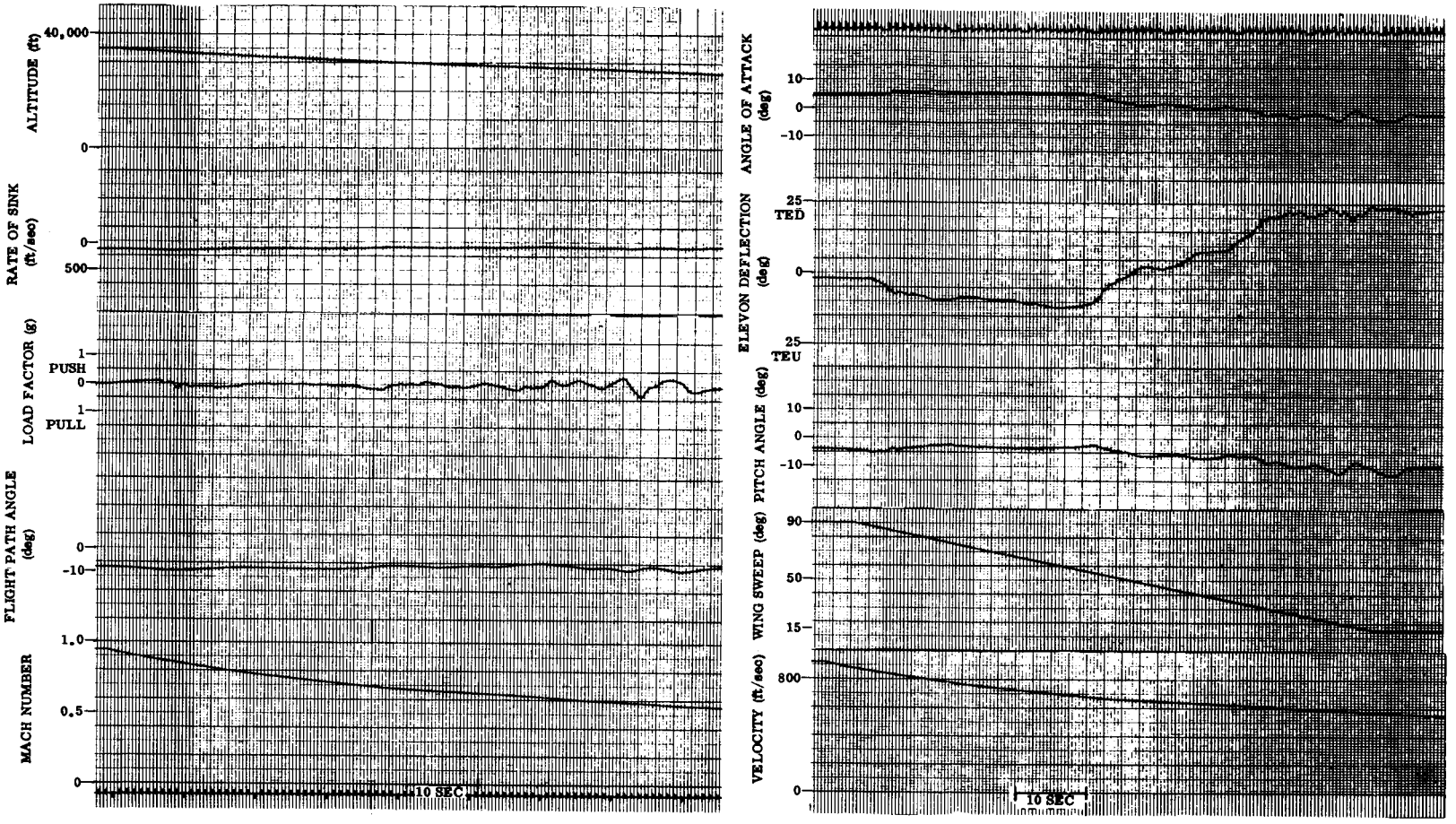

Figure 5-11. Wing Deployment; M = 0.95, H = 35,000 Ft, $\dot{\Lambda}$ = 1 deg/sec

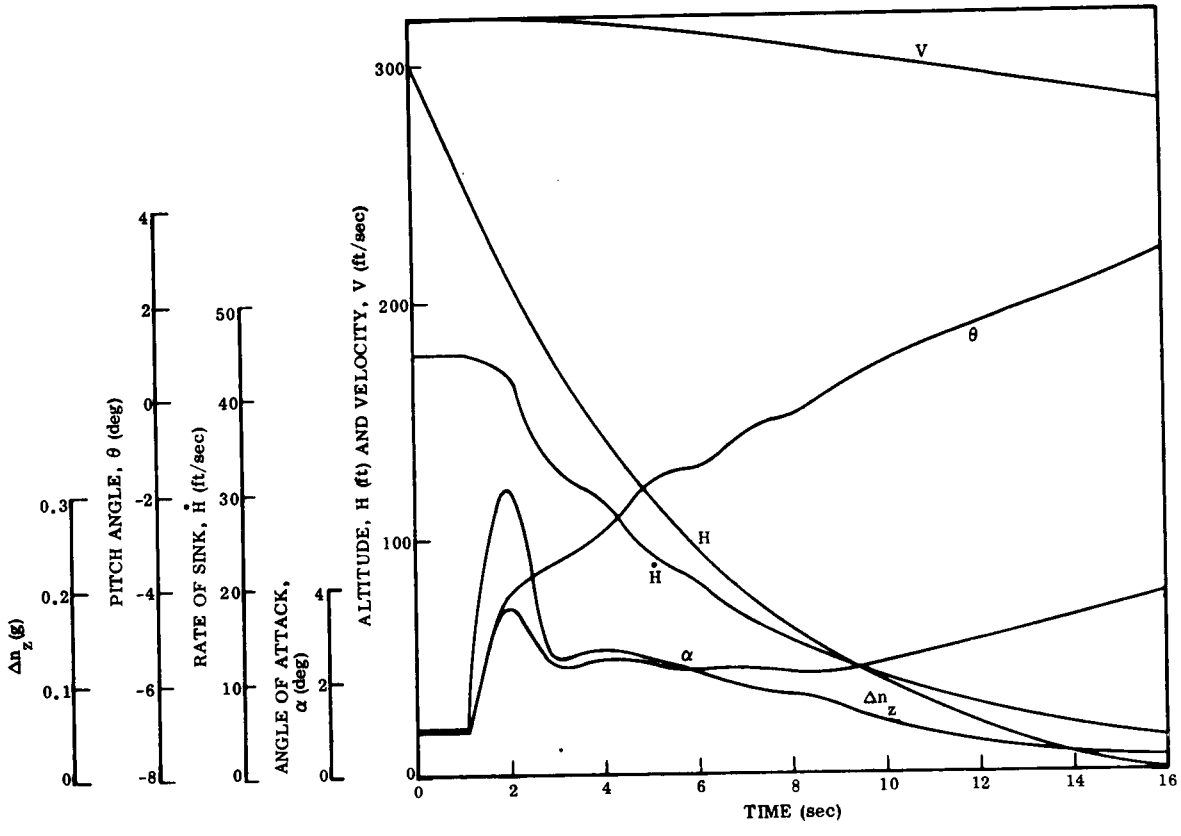

Figure 5-12. Landing Maneuver

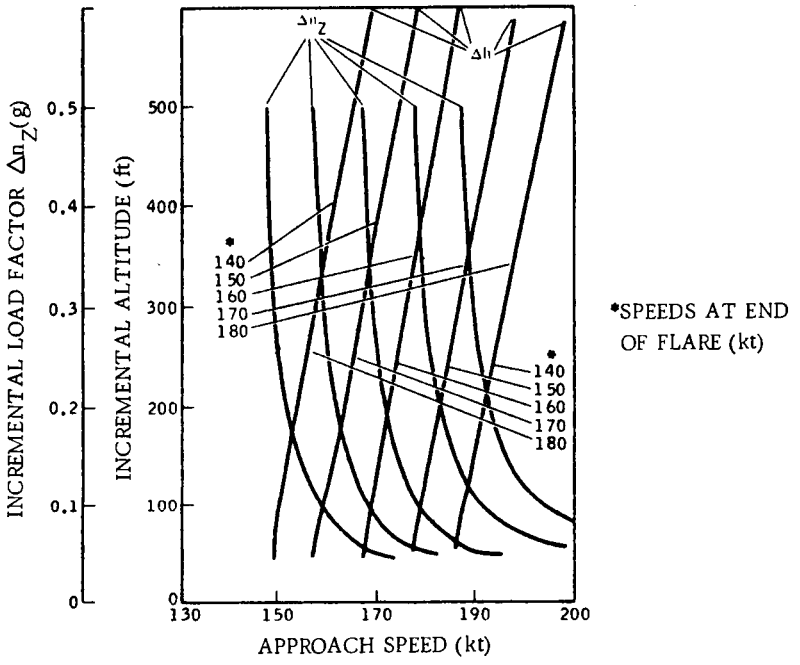

Figure 5-13. Summary of Vehicle Landing Characteristics

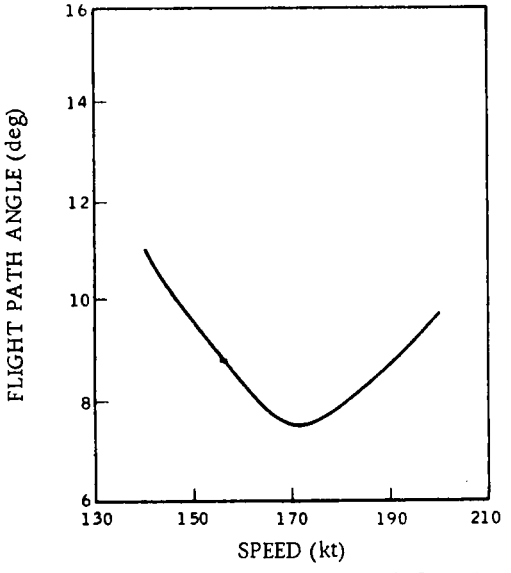

Figure 5-14. Equilibrium Glide Flight Path Angle Versus Speed

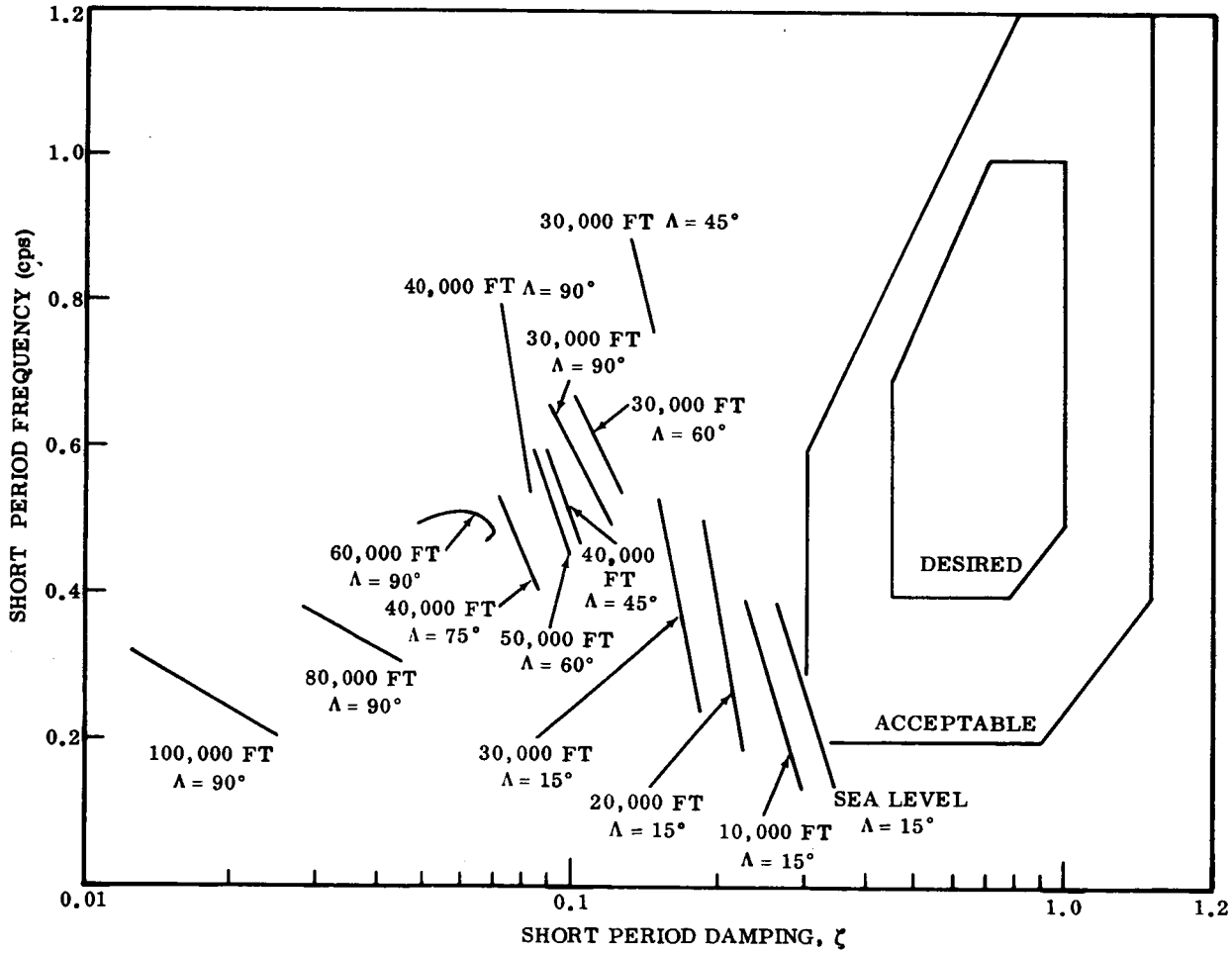

Figure 5-15. Short Period Frequency and Damping — No Augmentation

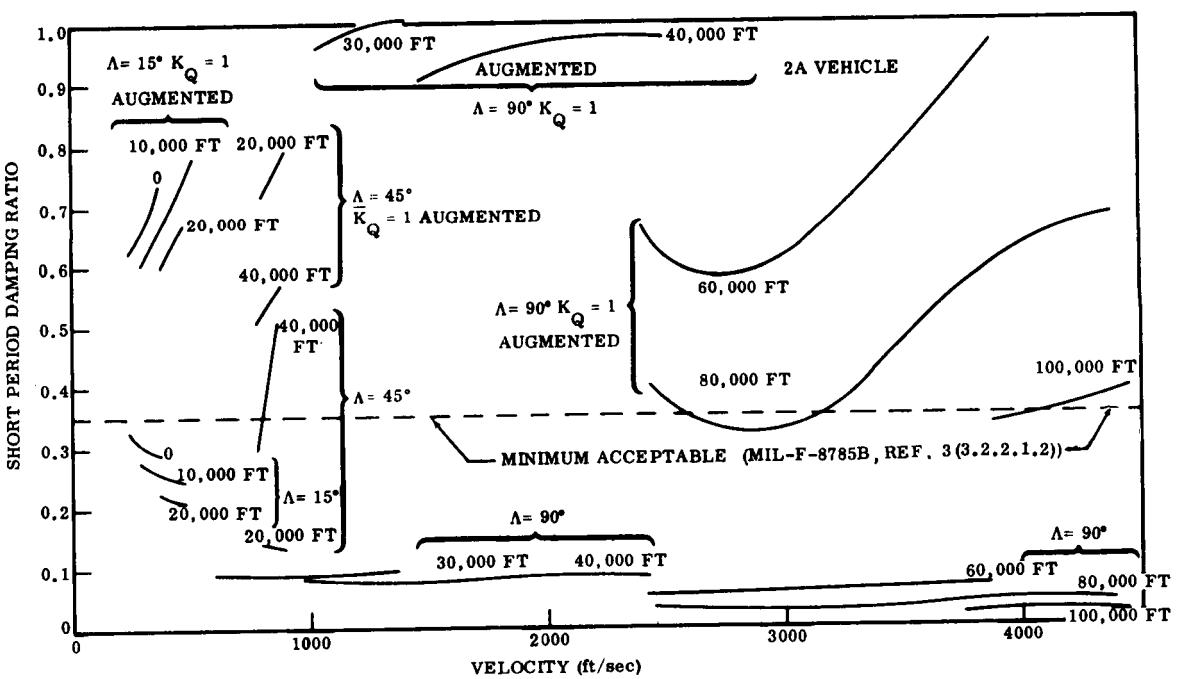

Figure 5-16. Short Period Damping Requirement

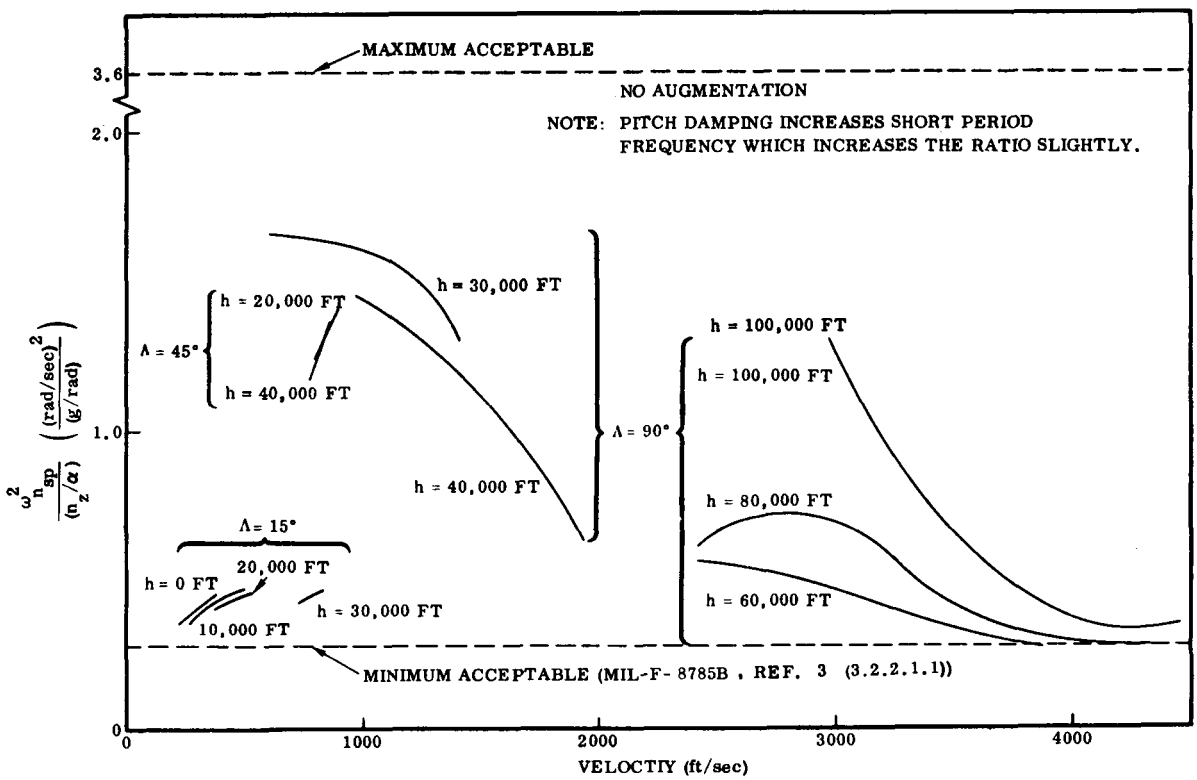

Figure 5-17. Short Period Frequency Requirement

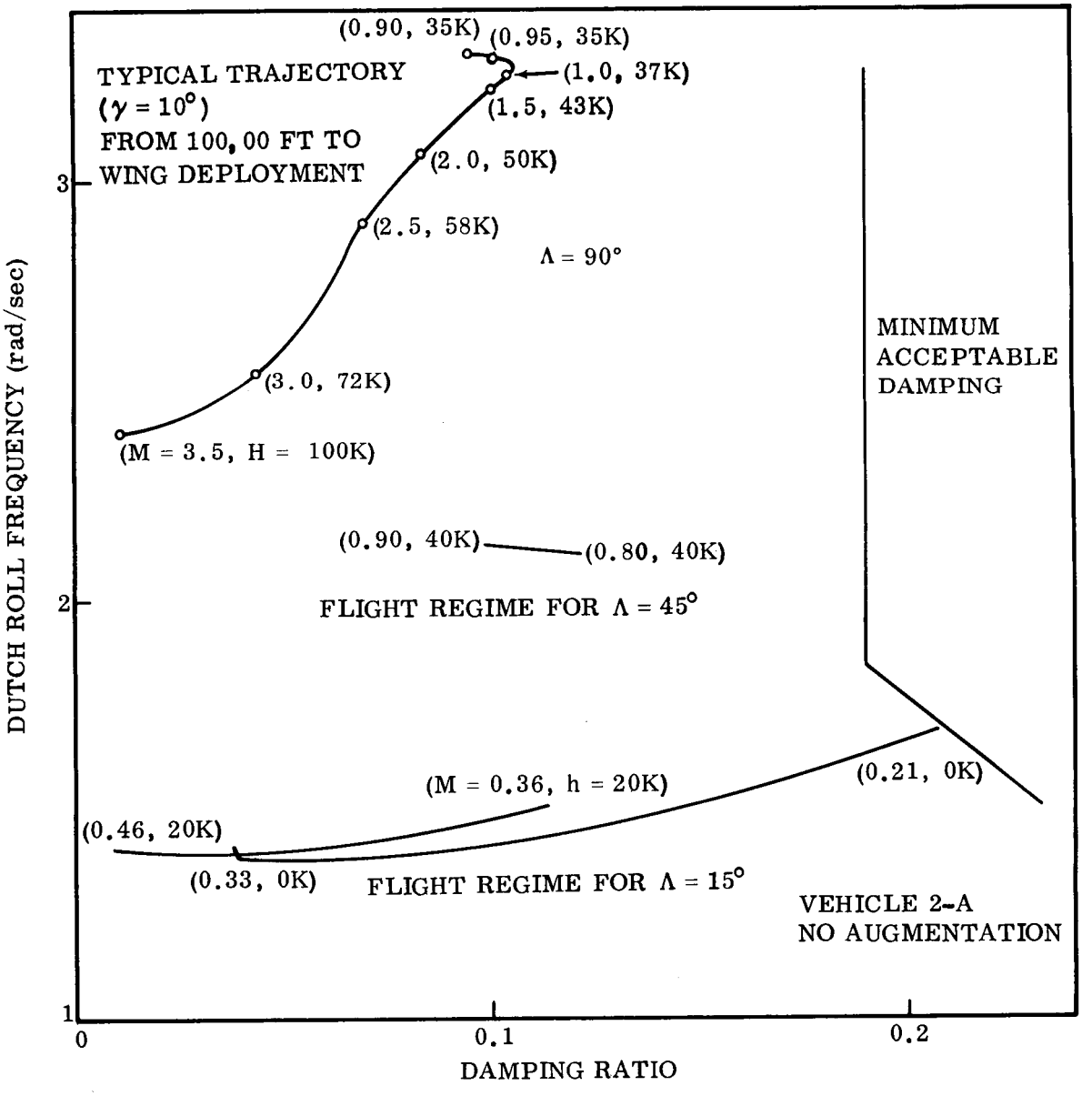

Figure 5-18. Dutch Roll Damping

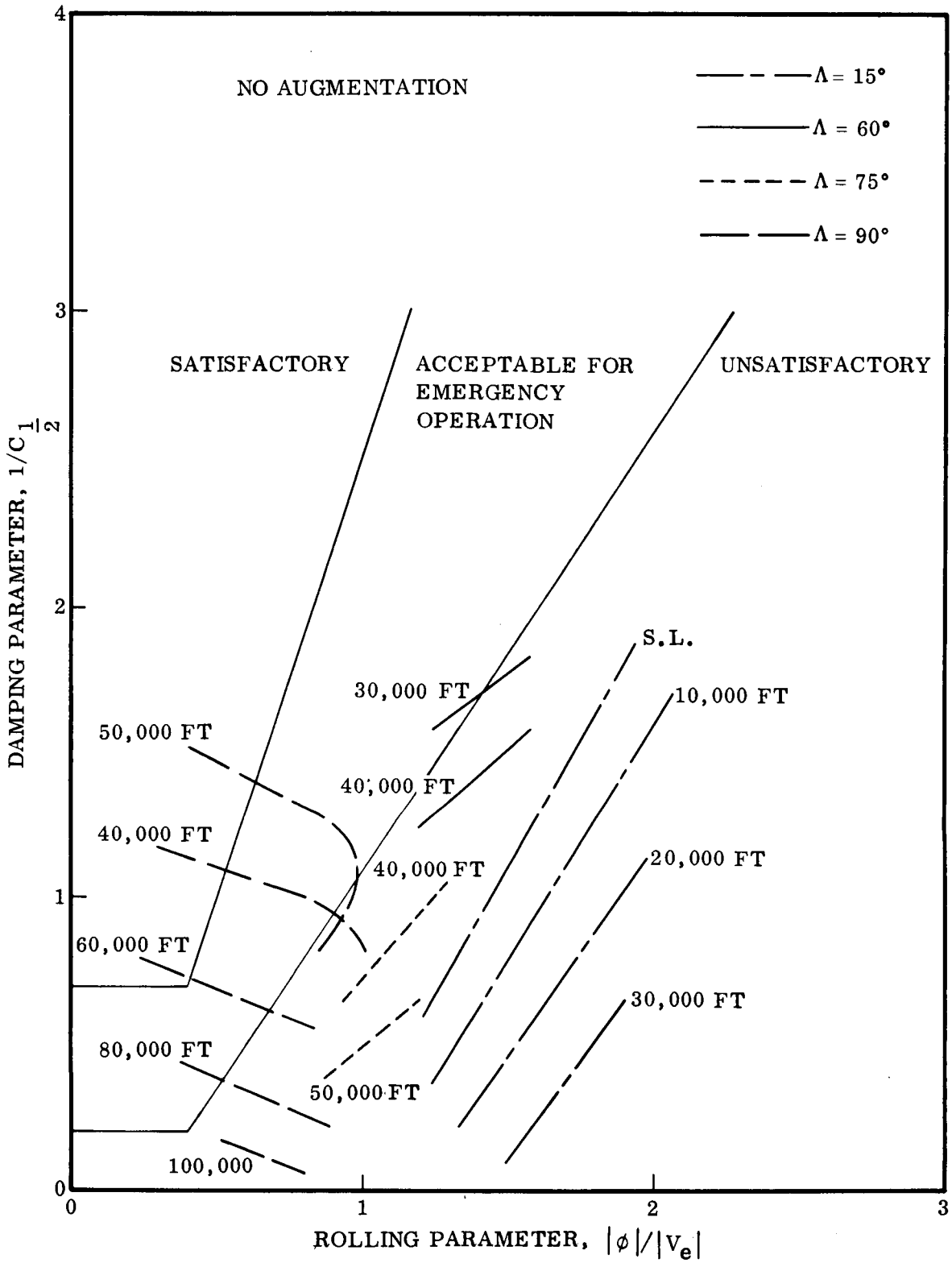

Figure 5-19. Roll to Sideslip Requirement

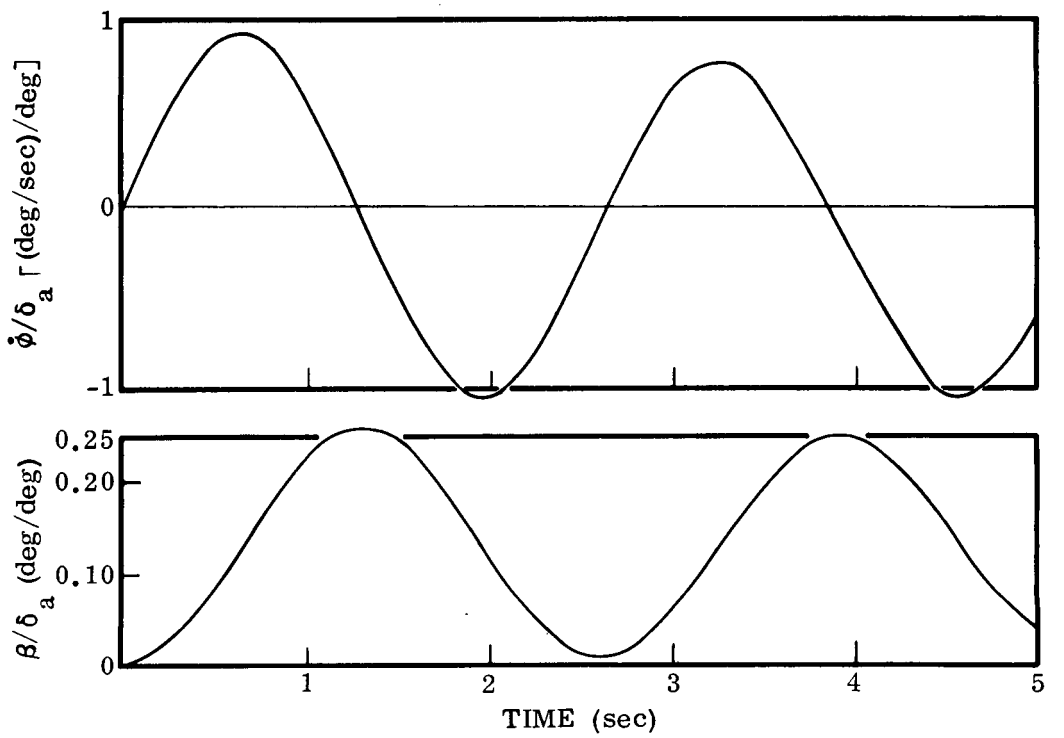

a. NO AUGMENTATION

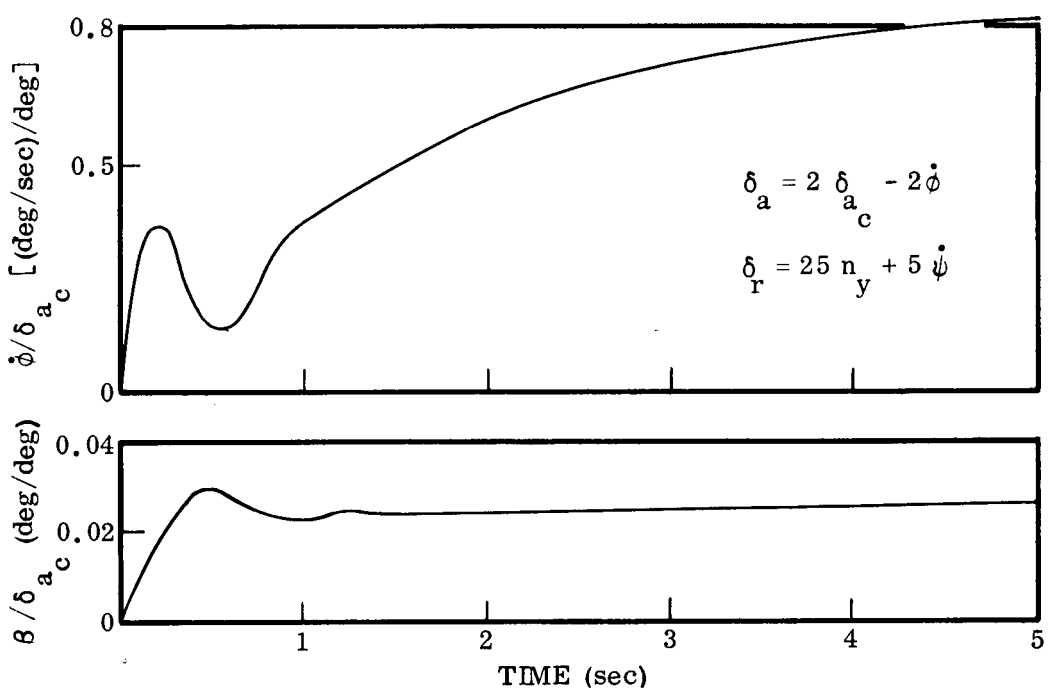

b. AUGMENTATION

Figure 5-20. Roll Response (M = 3.5, H = 100K), $\Lambda = 90°$

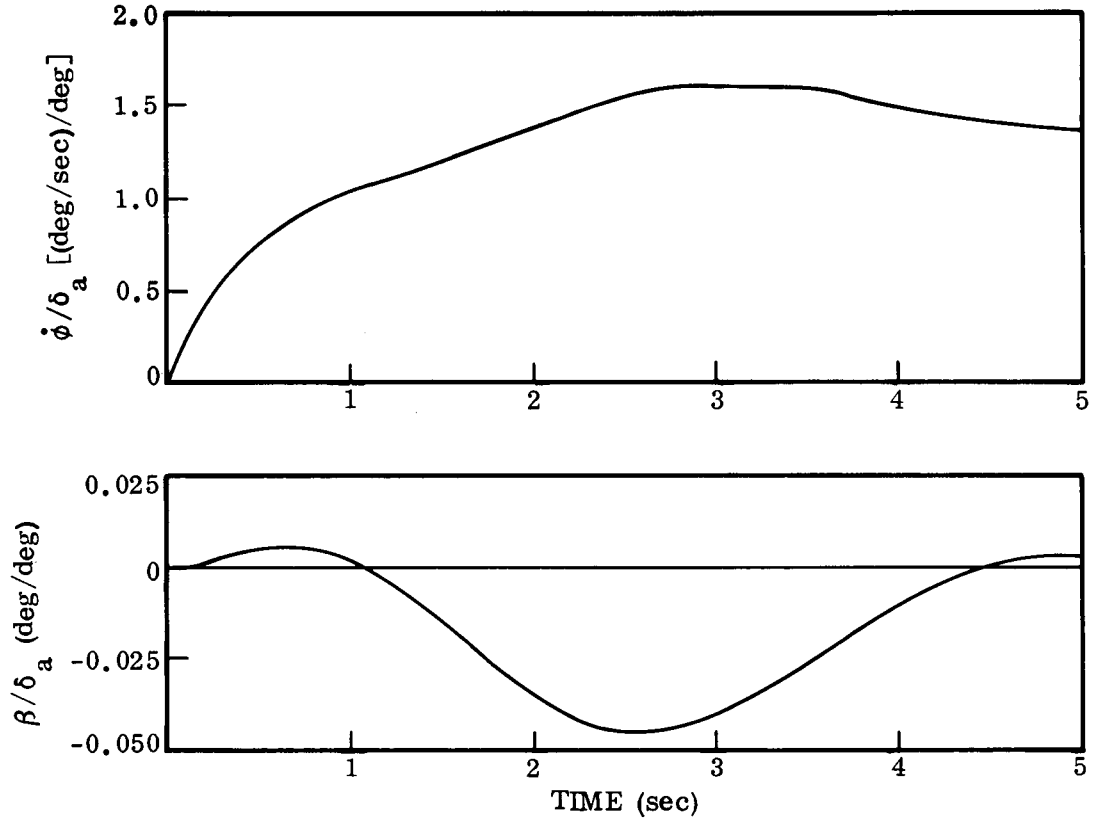

a. NO AUGMENTATION

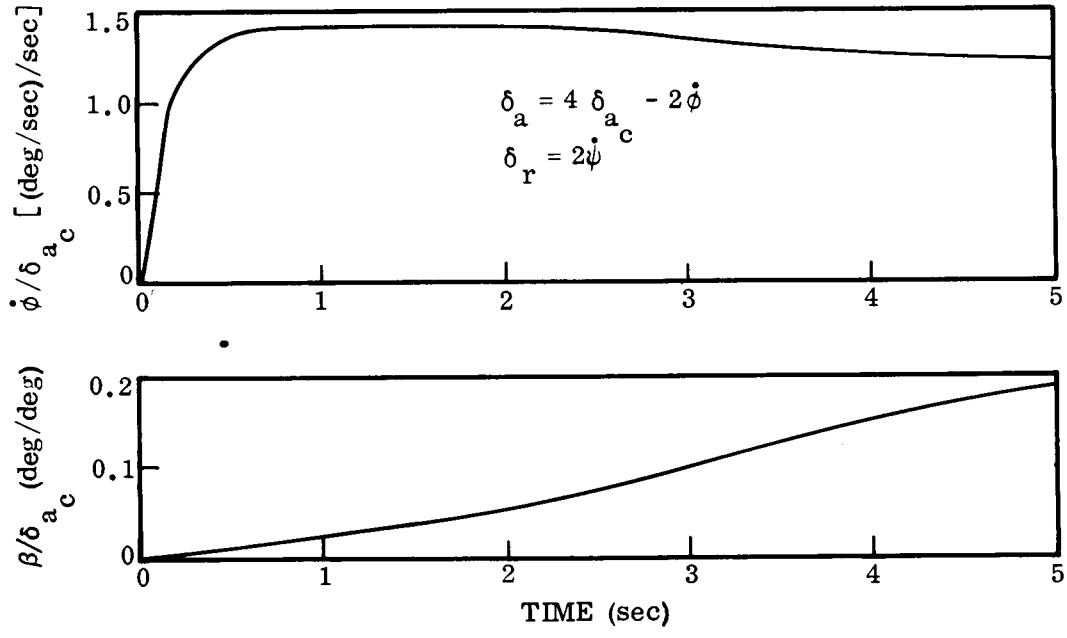

b. AUGMENTATION

Figure 5-21. Roll Response (M = 0.21, Sea Level), Λ = 15°